From the Department of Molecular Medicine and Surgery
Karolinska Institutet, Stockholm, Sweden

STUDIES OF SNAP-25 IN REGULATED MEMBRANE FUSION; METABOLIC CONSEQUENCES AND TUNING OF INTRACELLULAR CA(2+) DYNAMICS IN BETA CELLS

Teresa Daraio

Karolinska Institutet

Stockholm 2017

Published by Karolinska Institutet.
Printed by AJ E-Print AB

ISBN 978-91-7676-832-7

Studies of SNAP-25 in regulated membrane fusion; metabolic consequences and tuning of intracellular Ca(2+) dynamics in beta cells

THESIS FOR DOCTORAL DEGREE (Ph.D.)

By

Teresa Daraio

Principal Supervisor:
Associate Professor Christina Bark
Karolinska Institutet
Department of Molecular Medicine and Surgery
Division of Growth and Metabolism

Co-supervisor(s):
Professor Kerstin Brismar
Karolinska Institutet
Department of Molecular Medicine and Surgery
Division of Growth and Metabolism

Professor Marjan Slak Rupnik
Medical University of Vienna
Center of Physiology and Pharmacology
University of Maribor
Faculty of Medicine, Institute of Physiology

Opponent:
Professor Anders Tengholm
Uppsala University
Department of Medical Cell Biology

Examination Board:
Associate Professor Christian Broberger
Karolinska Institutet
Department of Neuroscience

Professor Per-Ola Carlsson
Uppsala University
Department of Medical Cell Biology

Professor Ingrid Dahlman
Karolinska Institutet
Department of Medicine, Huddinge
Unit of Endocrinology and Diabetes

“Above all, don't fear difficult moments. The best comes from them.”
Rita Levi-Montalcini

ABSTRACT

Increased release of insulin is usually regarded as a symptom of metabolic syndrome, contributing to insulin resistance in peripheral organs thus affecting glucose and insulin homeostasis. The existing animal models to address the metabolic syndrome are currently not optimal. In neuronal, neuroendocrine and endocrine cells, stimulus-dependent membrane fusion occurs via the SNARE complex, formed by the membrane-associated proteins SNAP-25 and syntaxin and the vesicle-associated protein VAMP-2, and requires intracellular Ca^{2+} elevations. The SNAP-25 protein exists as two splicing variants, SNAP-25a and SNAP-25b, differing in only 9 out of 206 amino acids. Both isoforms can mediate membrane fusion but their specific functions still remain unknown.

In this thesis, we have investigated if an apparently small modification in the exocytotic machinery could act as triggering factor for development of metabolic syndrome. We used a genetically modified mouse expressing normal levels of SNAP-25, but with only the SNAP-25a isoform available. In Paper I, by monitoring a number of metabolic parameters during 7 weeks on control or Western (high fat/high sucrose) diet, we found that SNAP-25b-deficiency leads to metabolic syndrome, characterised by hyperinsulinemia, obesity, hyperglycaemia, liver steatosis and adipocyte hypertrophy. These conditions were even more pronounced when the mutation was combined with Western diet. The metabolic phenotype caused by SNAP-25b-deficiency was accompanied by increased insulin secretion from the islets of Langerhans partially involving beta cell hyperplasia in a sex dependent manner. In Paper II we addressed these issues closer and focused on islet physiology by monitoring intracellular Ca^{2+} dynamics in beta cells upon glucose stimulation. SNAP-25b-deficiency impaired the collective control of Ca^{2+} oscillations in beta cells with early initiation and delayed termination of activity as well as decreased synchronicity. Derangements of intracellular Ca^{2+} oscillatory patterns can be related to the increased insulin secretion found in SNAP-25b-deficient mice. In Paper III we observed that the SNAP-25 isoforms mediate different interactions with proteins important for the strict control of exocytosis both in neurons and beta cells, such as Munc18-1 and the Gβγ subunits of the heterotrimeric G proteins.

In summary, we have shown that even a small modification in the machinery regulating membrane fusion, such as replacing SNAP-25b with SNAP-25a, acts as a triggering factor for the development of metabolic syndrome in mice. This condition was associated with loss of preciseness of Ca^{2+} oscillations in beta cells and increased insulin secretion. Thus, we propose the SNAP-25b-deficient mouse as a new model of metabolic syndrome and prediabetes.

LIST OF SCIENTIFIC PAPERS

I. Valladolid-Acebes I, **Daraio T**, Brismar K, Harkany T, Ögren SO, Hökfelt TG, Bark C. Replacing SNAP-25b with SNAP-25a expression results in metabolic disease. Proc Natl Acad Sci U S A. 2015; 112(31): E4326-4335.

II. **Daraio T**, Križančić Bombek L, Gosak M, Valladolid-Acebes I, Skelin Klemen M, Refai E, Berggren PO, Brismar K, Slak Rupnik M, Bark C. SNAP-25b-deficiency increases insulin secretion and changes spatiotemporal profile of Ca^{2+} oscillations in β cell networks. Sci Rep. 2017;7(1):7744.

III. **Daraio T**, Valladolid-Acebes I, Brismar K, Bark C. SNAP-25a and SNAP-25b mediate different interactions with Munc18-1 and Gβγ subunits (Manuscript).

PUBLICATIONS NOT INCLUDED IN THE THESIS

I. Valladolid-Acebes I, **Daraio T**, Brismar K, Hökfelt TG, Bark C. Minor differences in the molecular machinery mediating regulated membrane fusion has major impact on metabolic health. Adipocyte 2016; 5(3):218-325.

CONTENTS

1 Introduction 1
1.1 Metabolic syndrome 1
1.1.1 What is the metabolic syndrome? 1
1.1.2 Tissues affected by metabolic syndrome 1
1.1.3 Mouse models vs humans 2
1.2 Regulated exocytosis 2
1.2.1 The process of exocytosis 2
1.2.2 The SNARE complex 4
1.2.3 SNAP-25 isoforms 4
1.2.4 Regulation of exocytosis by other proteins 6
1.3 The pancreatic islet 7
1.3.1 Cell composition and exocrine pancreas 7
1.3.2 Stimulus-secretion coupling in beta cells 8
1.3.3 Modes of insulin secretion 9
1.3.4 Ca^{2+} dynamics in beta cells 9
2 Aims 11
3 Materials and methods 12
3.1 *In vivo* experiments 12
3.1.1 Animals 12
3.1.2 Diet 12
3.1.3 Measurement of metabolic parameters 12
3.1.4 Feeding pattern and caloric intake 13
3.1.5 Glucose tolerance tests and serum insulin levels 13
3.2 *Ex vivo* experiments 14
3.2.1 Total pancreas insulin content 14
3.2.2 Body fat distribution 14
3.2.3 Leptin and ghrelin in serum 14
3.2.4 Triglycerides content in liver 14
3.2.5 Isolation and cultivation of islets of Langerhans 15
3.2.6 Dynamic insulin secretion assay 15
3.3 Histology and immunohystochemistry 15
3.3.1 Adipocyte size quantification 15
3.3.2 Oil red “O” staining in liver 16
3.3.3 Analysis of islets parameters 16
3.3.4 Proximity ligation assay 17
3.4 Protein analyses 18
3.4.1 Western blotting in hypothalamus and liver 18
3.4.2 Western blotting and immunoprecipitation in hippocampus 18
3.4.3 Mass spectrometry 19
3.5 Electrophysiology and Ca^{2+} imaging in beta cells 20
3.5.1 Pancreatic tissue slice preparation 20

3.5.2 Electrophysiology 20
3.5.3 Loading of dyes and imaging of $[Ca^{2+}]_i$ oscillations in beta cells 21
3.5.4 Synchronization and functional connectivity of beta cells 22
3.6 Statistical analyses 23
3.7 Schematic methodological approach 23
4 Results and discussion 25
4.1 Paper I 25
4.1.1 SNAP-25b-deficient mice develop obesity and impaired insulin and glucose homeostasis 25
4.1.2 SNAP-25b-deficient mice display altered eating habits correlated to hypothalamic dysfunctions 26
4.1.3 SNAP-25b-deficiency leads to adiposity accumulation and dyslipidaemia 27
4.1.4 SNAP-25b-deficiency induces liver dysfunction 28
4.2 Paper II 28
4.2.1 SNAP-25b-deficiency increases insulin secretion and affects islet morphology 29
4.2.2 SNAP-25b-deficiency does not influence Ca^{2+}-sensitivity or rate of exocytosis 29
4.2.3 SNAP-25b is necessary for accurate regulation of Ca^{2+} dynamics in beta cells 30
4.3 Paper III 31
5 Conclusions 34
6 Acknowledgements 35
7 References 39

LIST OF ABBREVIATIONS

AMPK	AMP-activated protein kinase
BMI	Body mass index
CoD	Control diet
Cx36	Connexin-36
DP	Depot pool
ER	Endoplasmic reticulum
ERK1/2	Extracellular signal-regulated kinase 1/2
GABA	Gamma-aminobutyric acid
GIRK	G-protein-coupled inwardly-rectifying K^+ channel
GPCR	G protein coupled receptor
GTT	Glucose tolerance test
H&E	Hematoxilin and eosin
HOMA	Homeostatic model assessment
LDCV	Large dense-core vesicle
LTD	Long-term depression
MT	Mutant
Munc18-1	Mammalian uncoordinated-18-1
NSF	N-ethylmaleimide-sensitive factor
ObR	Leptin receptor
ORO	Oil red “O”
RP	Releasable pool
RRP	Ready releasable pool
SERCA	Sarcoendoplasmic reticulum Ca^{2+} transport ATPase
SG	Secretory granule
SLMV	Synaptic-like micro vesicle
SM	Sec1/Munc18-like
SNAP-25	Synaptosomal-associated protein 25
SNAP-α	N-ethylmaleimide-sensitive factor attachment protein α
SNARE	Soluble NSF attachment protein receptor
SRP	Slowly releasable pool

STAT3	Signal transducer and activator of transcription 3
SV	Synaptic vesicle
T2D	Type 2 diabetes
UPP	Unprimed pool
VAMP	Vesicle-associated membrane protein
VDCC	Voltage-dependent Ca^{2+} channel
WeD	Western (high fat/high sucrose) diet
WT	Wild type

1 INTRODUCTION

1.1 METABOLIC SYNDROME

1.1.1 What is the metabolic syndrome?

The metabolic syndrome is a cluster of several metabolic abnormalities, such as hyperinsulinemia, central obesity, insulin resistance, elevated blood pressure, impaired fasting glucose and/or glucose tolerance and dyslipidaemia [1]. All these risk factors appear to be influenced by both genetic background and environmental influences. Individuals with metabolic syndrome have a five-fold increased risk of developing type 2 diabetes (T2D) [2].

1.1.2 Tissues affected by metabolic syndrome

During development of the metabolic syndrome, many tissues are affected, mainly the brain, liver, pancreas, adipose tissue and muscle.

An improper metabolic control can originate from impaired **brain** sensing of energy balance and integration of feedback signals from the periphery. Neuronal nuclei involved in the sensation of adiposity, satiety and glucose are highly concentrated in the hypothalamus, which is currently an important area of investigation [3]. Progressing hyperinsulinemia and hyperleptinemia result in an impaired sensation or transduction in hypothalamic neurons (insulin/leptin resistance), ultimately leading to increased food intake. Alterations in neuronal intracellular metabolism, such as mitochondrial dysfunctions and endoplasmic reticulum (ER) stress, also contribute to the metabolic disease state [4].

The altered secretion of adipokines during the metabolic syndrome causes ectopic lipid deposition in the **liver**. This excessive storage causes an intracellular pro-inflammatory state, giving rise to a variety of liver pathologies from mild hepatosteatosis (or fatty liver disease) to non-alcoholic steatohepatitis. Hepatic insulin resistance affects intracellular signalling pathways, leading to increased hepatic glucose production, a hallmark of T2D [5].

Insulin resistance leads to compensatory increases in insulin release from **beta cells** within the islets of Langerhans. Chronic hyper production of insulin in beta cells causes beta cell expansion (or "islet hypertrophy"), resulting in enlarged islets in the pancreas [6]. When insulin resistance progresses, the effects of insulin in target tissues diminishes and beta cells progressively fail to release sufficient amount of insulin. T2D is characterised by a complete loss of the first phase of insulin secretion and diminished second phase (described in 1.3.3) [7,8].

In the presence of excessive caloric intake, the **adipose tissue** expands as a result of adipocyte hypertrophy and hyperplasia. The adipocytes challenged by metabolic syndrome are characterised by high degree of inflammation and insulin resistance which turns out to stimulate lipolysis and increase the storage of lipids in non-adipose tissues. The release of adipokines is compromised, with elevated leptin levels and diminished adiponectin levels [9,10].

Insulin resistance in skeletal **muscle** is an important factor in the pathogenesis of T2D. It can be mostly attributed to defects in insulin signalling and glucose transport which results in decreased glycogen synthesis. Possible causes of this phenomenon include ectopic lipid accumulation in myocytes, changed release of adipokines associated with inflammation and intracellular accumulation of reactive oxygen species (ROS) [11,12].

1.1.3 Mouse models vs humans

The metabolic syndrome is dramatically increasing worldwide and the International Diabetes Federation (IDF) has estimated that 20-25% of the population is affected by the disease. It is therefore crucial to experimentally study causes and progression of metabolic impairments. A major issue when studying mouse models is that none can mimic all the aspects of the human metabolic syndrome. Most of the models used for the study of obesity arose from spontaneous mutations in the leptin or leptin receptor gene ($Lep^{ob/ob}$ and $LepR^{db/db}$ mice) and although they develop a metabolic phenotype close to the human syndrome (obesity, insulin resistance, glucose intolerance and hepatic steatosis), similar mutations in humans are very rare [13].

So far, the best model to resemble the human metabolic syndrome and for testing potential therapeutic interventions is chronic consumption of a high fat/high sucrose diet.

1.2 REGULATED EXOCYTOSIS

1.2.1 The process of exocytosis

Exocytosis is the cellular process by which certain substances packed into vesicles can be released outside the cell by fusion with the plasma membrane. It requires the interplay of different proteins and mechanisms depending on the cellular type but overall the process is highly conserved in eukaryotic cells [14]. Exocytosis exists as constitutive and regulated and they both require expenditure of energy. Constitutive exocytosis is a continuous, rather slow, process performed by all cells for delivering newly synthetised (membrane) proteins to be incorporated in the plasma membrane or components released to build the extracellular matrix. Regulated exocytosis is modulated by secretagogues and allows a rapid and massive

release after physiologically appropriate stimuli and is preceded by influx of extracellular Ca^{2+}. It occurs only in specialised secretory cells such as neurons, endocrine and neuroendocrine cells [15]. In neurons regulated exocytosis is achieved through two types of vesicles: small synaptic vesicles (SVs), usually at the nerve terminal containing acetylcholine, catecholamine and glutamate and large dense-core vesicles (LDCVs), transporting condensed proteins and peptides. In endocrine and neuroendocrine cells, fast exocytosis is achieved by synaptic-like microvesicles (SLMVs), larger than SVs, whereas slow exocytosis occurs through secretory granules (SGs) (endocrine cells) and LDCVs (neuroendocrine cells) [16,17]. SVs are smaller (diameter < 30nm) compared to LDCVs (hundreds of nm) and mediate exocytosis at least one order of magnitude faster than LDCVs, requiring higher intracellular Ca^{2+} concentrations, $[Ca^{2+}]_i$ [18–20].

The vesicles can be classified into different pools, depending on their release capability and kinetics of fusion [21,22]. There are two releasable pools of vesicles: the first one comprises the fast burst component and belongs to the ready releasable pool (RRP), the slow burst component is built by the fusion of the slowly releasable pool (SRP). The releasable pools are refilled from the unprimed pool (UPP) during "priming" (see below) and account for the sustained component of exocytosis. At last, the depot pool (DP) represents the largest pool in adrenal chromaffin cells where the vesicles are used to refill the UPP upon depletion during "docking" step (see below) [22].

During regulated membrane fusion, the vesicles undergo a number of biochemical steps that will eventually lead to fusion with the plasma membrane. These stages are classified into docking, priming and fusion (Figure 1). The docking corresponds to the transfer of vesicles from the DP to the UPP and their allocation in proximity of the plasma membrane (or active zone for SVs). During the priming process, UPP are transferred to a releasable pool (RP) stage with the formation of the trimeric SNARE complex [23,24]. Finally the fusion process occurs when the vesicle either collapses with the plasma membrane ("full collapse" fusion) or a small fusion pore opens for releasing part of the vesicle content and then closes ("kiss-and-run" fusion) [22,25].

Membrane fusion is achieved with a concomitant entry of Ca^{2+} via the opening of voltage-dependent Ca^{2+} channels (VDCCs). The raise in $[Ca^{2+}]_i$ initiates signal transduction with short and long term effects on secretion, for example by activating protein kinases or by inducing direct interactions between exocytic proteins located in the vesicle membrane and those situated in the plasma membrane [26–29].

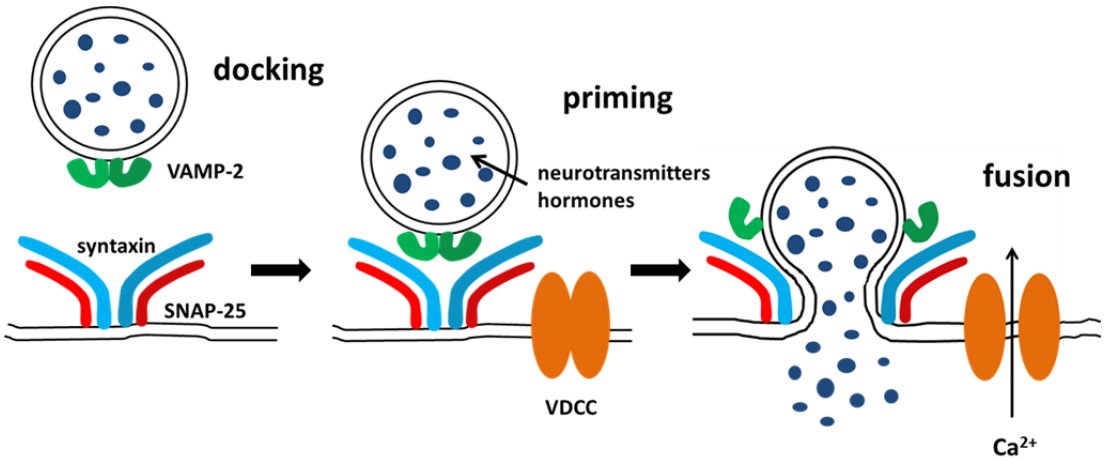

Figure 1. Schematic mechanisms of regulated membrane fusion. During docking the vesicle/granule approaches the plasma membrane and during priming the assembly of the SNARE complex occurs. Membrane fusion is triggered when Ca^{2+} enters the cell via VDCCs.

1.2.2 The SNARE complex

A vesicle fusion event requires many coordinated and regulated steps. Rothman, Schekman and Südhof have been pioneers for the discovery of proteins necessary for this process [24,30,31]. The SNARE complex acts as a conserved core protein machinery for all membrane fusion events. Syntaxin, SNAP-25 and VAMP (also called synaptobrevin) were the first SNAREs to be discovered [32–34]. Syntaxin and VAMP are anchored to membranes by C-terminal transmembrane domains, whereas SNAP-25 is attached through post-translational palmitoylation of four cysteine residues in its central region [35,36]. All SNARE proteins are characterised by a ~70 residue "SNARE motif" with heptad repeats that forms coiled-coil structures. The SNARE core complex has a four-stranded coiled-coil structure, one coil from syntaxin and VAMP and two from SNAP-25. This structure, called "*trans*-SNARE complex", bridges vesicles and plasma membranes close to each other and catalyses fusion. In the course of fusion, the *trans*-conformation is adjusted to a *cis*-SNARE conformation with all SNAREs located on the same membrane [37]. The complex is highly stable and to dissociate it requires ATP and two proteins: NSF and its adaptor protein, SNAP-α [14,38].

1.2.3 SNAP-25 isoforms

Mice deficient of SNAP-25 exhibit embryonic lethality and evoked synaptic transmission is abolished, although they show an early nervous system development and spontaneous transmitter release [39]. SNAP-25 is expressed as two splicing variants, SNAP-25a and SNAP-25b, which originate from two divergent versions of exon 5. They differ in only 9 out of 206 amino acids (Figure 2) corresponding to a central domain of the protein spanning the quartet

of cysteine residues that are substrates for palmitoylation and three residues that are part of the N-terminal SNARE motif [35,36,40,41].

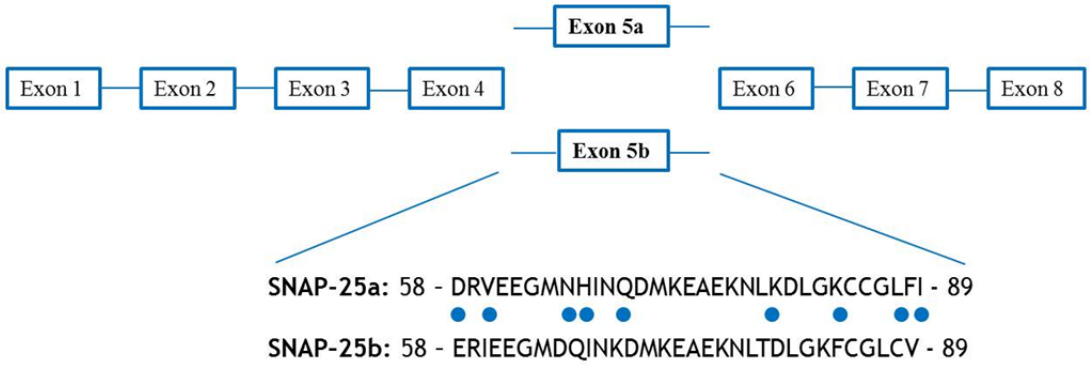

Figure 2. Schematic structure of the *Snap25* gene and amino acids sequence encoded by exons 5a and 5b.

Both SNAP-25a and SNAP-25b can participate in the core SNARE complex [42]. The expression levels of the two isoforms are developmentally and spatially regulated. In rodent brain, SNAP-25a is more abundant during early development, but by the second postnatal week SNAP-25b becomes the predominant isoform [43,44]. SNAP-25a expression remains in specific brain regions, such as cortical and hypothalamic structures, and in endocrine and most neuroendocrine cells SNAP-25a is the dominant isoform also in adulthood [43,45–47]. Normal expression levels of total SNAP-25 are essential for controlled synaptic function [48,49] and downregulation leads to defects in SNARE complex assembly and synaptic plasticity [48,50]. The functional difference between the two splice variants has not been fully clarified. What is currently believed is that SNARE complexes containing SNAP-25b are more stable, thus increasing the pools of primed vesicles [42,51,52]. Recently, a point mutation in SNAP-25b carried by a viable mouse mutant, has been associated with impairments in vesicle trafficking and regulated membrane fusion, likely dependent on failure to mobilise new vesicles from the RP [53]. Moreover, SNAP-25 has been found to interact and modulate the activity of Ca^{2+} channels [54–56]. The C-terminus of SNAP-25 inhibits L-type Ca^{2+} currents in beta cell whereas the rest of the protein stimulates channel activity [54]. Interestingly, it was recently demonstrated that the SNAP-25b isoform together with syntaxin 1 was more efficient in inhibiting VDCC currents in chromaffin cells than SNAP-25a [56].

1.2.4 Regulation of exocytosis by other proteins

1.2.4.1 Munc18-1

Munc18-1 belongs to a group of proteins called SM proteins (Sec1/Munc18-like) initially identified in genetic screens in yeast [57]. It has been linked to membrane fusion since it was first isolated bound to syntaxin 1 [31]. The SM proteins are essential for all types of intracellular membrane fusion where also SNAREs are involved and their absence leads to blockage of fusion [14] and neurotransmitter release in Munc18-1 knockout mice [58]. The general function of Munc18-1 is still under debate because it probably performs multiple roles. SM proteins are equipped with a conserved ~600-amino acid sequence that folds into an arch shape and binds the closed conformation of syntaxin 1 [59,60]. This binding with syntaxin 1 disables the formation of the SNARE complex. Munc18-1 does not always act as a negative modulator of membrane fusion but is also required for all fusion events. More recently, a second mechanism of interaction between Munc18-1 and SNAREs was found, explaining how it could promote fusion [61,62]. Here, the SM protein is anchored to the N-terminal peptide of syntaxin, thus leaving its arch-shaped body to fold back on the SNAREpin and clasp across the zippering four-helices near the plasma membrane. Thus, SM proteins would act as catalysts for SNAREs, which in turn catalyses the membrane fusion event [14].

1.2.4.2 Heterotrimeric G proteins

Major modulators of neurotransmitter/hormone action are the G protein coupled receptors (GPCRs), which consist of seven transmembrane α-helices [63]. Despite the elevated number of GPCRs, they are coupled with relatively few heterotrimeric G proteins (α, β and γ subunits). The heterotrimers are categorised into four families: G_s, $G_{i/o}$, G_q, $G_{12/13}$, based on the functional similarity of the α subunit [64]. When the ligand binds, the receptor activates the attached G protein which dissociates into one α subunit and a βγ-complex. Gα can diffuse along the membrane surface to activate/inhibit target proteins, often enzymes that generate second messengers. The βγ-complex works as a functional monomer also able to affect protein activity [63]. $G_{i/o}$-coupled receptors ($5HT_1$ serotonin receptors, α_{2A} adrenergic receptors, D_2 dopamine receptors, M_4 muscarinic receptors, opioid receptors, etc.) on both pre- and postsynaptic sites protect against overstimulation by releasing G protein βγ subunits. These subunits act both postsynaptically by activating G-protein-coupled inwardly-rectifying K^+ (GIRK) channels and presynaptically by inhibiting VDCCs [65,66] or by regulating GIRK channels [67]. Ultimately they interact with one or more components of the exocytotic machinery [63].

The first evidence for the latter function of the βγ subunits came from studies on lamprey reticulospinal motor neuron synapses where Gβγ inhibition was mediated via the C-terminal region of SNAP-25 and the Gβγ subunits directly interacted with the SNARE complex proteins in *in vitro* binding assays [68–71]. It was also noted that the syntaxin and SNAP-25 domains interacting with Gβγ were functionally important for Ca^{2+}-dependent synaptotagmin binding [71]. Therefore, it was predicted that at low intracellular Ca^{2+} concentrations, Gβγ binding to the SNAREs predominates, but when Ca^{2+} concentration increases synaptotagmin competes with Gβγ, blocking inhibition and allowing exocytosis (Figure 3) [71].

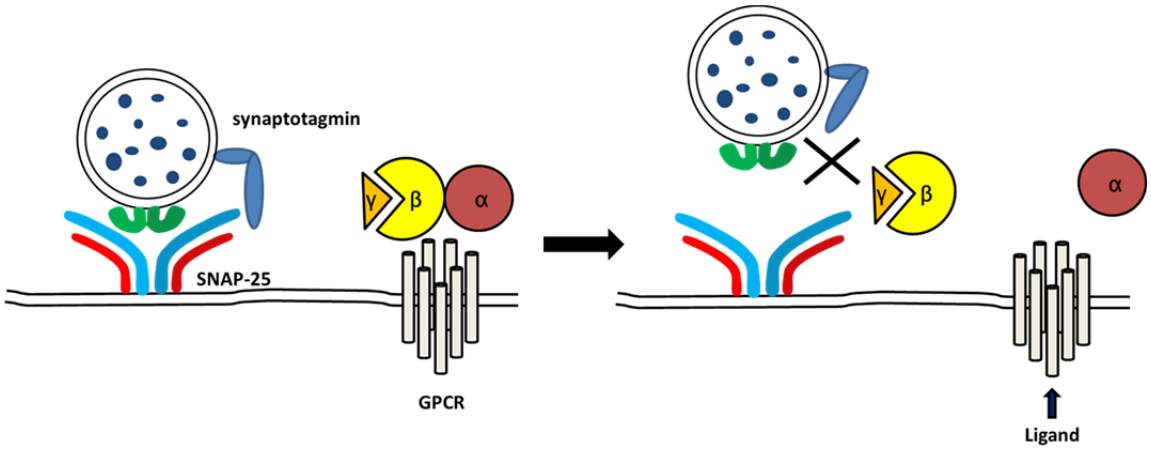

Figure 3. Schematic mechanisms of presynaptic inhibition modulated by the Gβγ subunits of the heterotrimeric G proteins. Upon ligand interaction with the GPCR, the Gβγ subunit competes with synaptotagmin for binding the exocytosis machinery, thus inhibiting fusion.

Inhibition of synaptic transmission via Gβγ is not only important for transient events, but it also plays a role in long-term alterations of presynaptic signals connected to long-term depression (LTD) [72]. Emerging evidence places LTD as fundamental process for modelling long-lasting changes in circuit function, learning, memory and behaviour [73]. Furthermore, a similar mechanism has been proposed for inhibition of insulin secretion in beta cells [74].

1.3 THE PANCREATIC ISLET

1.3.1 Cell composition and exocrine pancreas

The discovery of the islets of Langerhans in the pancreas dates back to 1869, when a German medical student, Paul Langerhans, observed cell-clusters disseminated in the rabbit pancreas [75]. They constitute the endocrine part of the pancreas which accounts for 1-2% of the total pancreatic volume. Islets are structurally defined cellular aggregates of a few to several thousand endocrine cells [76]. The islet comprises at least 5 types of polypeptide-hormone-

secreting endocrine cells and the majority belongs to the population of beta cells (60-80%) which secrete insulin, the only blood glucose lowering hormone. Second in number are the alpha cells (10-20%), which produce glucagon. Delta cells and PP cells (5%) release somatostatin and pancreatic polypeptide, respectively, and finally the epsilon cells (1%) which secrete ghrelin [77,78]. The intraislet organization of endocrine cells differs among species: in rodents, the islet core is primarily composed of beta cells while the other cell types are localised peripherally, in humans all types of cells are intermingled with no obvious patterns of organization [79,80,78]. The close arrangement of islet cells facilitates intercellular coupling and paracrine interactions [81].

The islets are embedded in the exocrine pancreas, organised in acini and formed by acinar cells which secrete enzymes for food digestion (α-amylase, lipase and proteases). Moreover, there exists an extensive cell-cell communication between the endocrine islet and the exocrine acinar cells via desmosomes and adherent junctions, which become structurally lost during remodelling changes associated with the development of T2D [82].

1.3.2 Stimulus-secretion coupling in beta cells

The pancreatic beta cell acts as a metabolic sensor, integrating nutrients, hormones and neurotransmitters stimuli to finally secrete insulin. The beta cell is equipped with two distinct types of secretory vesicles, the SLMVs containing gamma-aminobutyric acid (GABA) and the SGs containing insulin [17].

Insulin is released following food digestion and glucose acts as the most important nutrient secretagogue for beta cells. Blood glucose enters the beta cell via a transporter (GLUT2 is the predominant in mice) and starts to be metabolised by phosphorylation, a reaction catalysed by the enzyme glucokinase. Once phosphorylated, glucose-6-phosphate, cannot exit the cell and undergoes a metabolic process involving the mitochondria and the release of energy in the form of ATP [83,84]. The increased ATP/ADP ratio promotes the closure of the ATP-sensitive K^+-channels (K_{ATP}-channels) in the plasma membrane. Since these channels maintain a resting potential of about -70 mV, their closure leads to a gradual depolarization of the cell. With changes in membrane potential, the VDCCs are activated with subsequent increase in cytosolic free Ca^{2+} and finally leading to exocytosis of insulin granules (Figure 4). It has been demonstrated that in beta cells L-type Ca^{2+}-channels bind the SNARE core complex via syntaxin, SNAP-25 and synaptotagmin with subsequent local increase of $[Ca^{2+}]_i$ triggering membrane fusion. The site of interaction on the channel is called “synprint” [55].

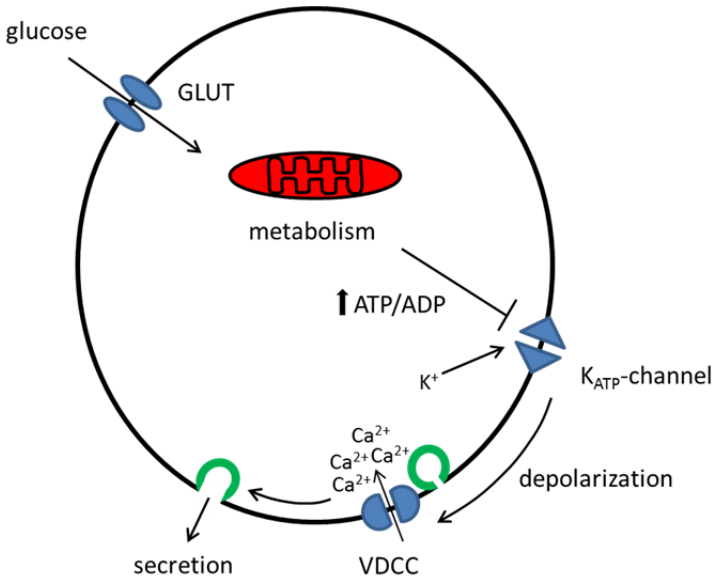

Figure 4. Schematic representation of glucose-stimulated insulin secretion in a beta cell. Glucose enters the cell via glucose transporters and is metabolised in the mitochondria with subsequent production of energy (ATP). Raise in ATP/ADP ratio closes the K_{ATP}-channels, depolarizing the cell membrane which will in turn open the VDCCs. Membrane fusion is triggered after Ca^{2+} enters the cell.

1.3.3 Modes of insulin secretion

Experiments in isolated pancreatic islets and hyperglycaemic clamps have demonstrated that glucose induces insulin secretion in a biphasic pattern: a fast and transient "first phase" followed by a sustained and long-lasting "second phase" [7,8,18]. Loss of the first phase and reduction of the second phase are traits of T2D whereas in obese individual both phases are increased [7,8]. During the last decades, many different theories have been suggested behind the molecular mechanisms of biphasic insulin secretion, yet without a final conclusion. However, the most prevailing hypothesis is that the release of the RRP of vesicles (5% of total content), docked on the plasma membrane, accounts for the first phase of insulin release and the second phase is build up by recruitment of a RP to the plasma membrane [8].

There are different modes of exocytosis besides the full fusion mode. The "kiss-and-run" fusion occurs when the granule-exocytotic machinery complex is not in proximity of VDCCs and therefore the fusion pore opens only transiently [85]. The "compound" exocytosis has been described to correspond to fusion of several granules organised in multivesicular complexes [85,86]. However, the physiological role of the different exocytotic modes and their possible involvement in metabolic disease and T2D is still not understood.

1.3.4 Ca^{2+} dynamics in beta cells

Ca^{2+} impacts nearly every aspect of cellular life. It acts as a secondary messenger controlling a number of processes such as secretion, apoptosis and gene expression. As previously

mentioned, Ca^{2+} plays a fundamental role for exocytosis in beta cells as it regulates trafficking, docking and initiates fusion of the insulin granules via the SNAREs proteins. Ca^{2+} influx into the cytoplasm has been described to occur rhythmically due to a rhythmic nature of the underlying electrical activity [87,88]. Ca^{2+} sequestration and release from the ER contributes to smoothing the oscillations observed in islets and it occurs under the fine regulation of the Ca^{2+} pumps present on the ER, such as the sarcoendoplasmic reticulum (SR) Ca^{2+} transport ATPase, SERCA [89]. Yet the exact patter of Ca^{2+} elevations depends on the experimental model employed. Two types of oscillations have been described until now: slow oscillations (3-5 min) recorded in single beta cells or cultured islets and fast oscillations (1-2 min) recorded in freshly isolated islets [90,91]. Also, an oscillatory pattern of insulin release, driven by oscillations of $[Ca^{2+}]_i$ has been demonstrated, suggesting a refined temporal correlation between electrical activity, Ca^{2+} signalling and insulin secretion in isolated islets [92,93]. Moreover, *in vivo* experiments have demonstrated similar $[Ca^{2+}]_i$ and membrane potential oscillations as the ones described in freshly isolated islets [94]. A considerable degree of synchronicity in electrical activity between different cells in the same islet has been shown along with $[Ca^{2+}]_i$ oscillations occurring synchronously across the islet [90,94–96]. This extensive communication among beta cells is achieved by means of the gap junction protein connexin 36 (Cx36), which allows exchange of small signalling molecules such as Ca^{2+} ions [97]. In several mouse models of diabetes [98–100], in Cx36-null mouse models [101,102] and also in humans with prediabetes [103] the loss of synchronization in $[Ca^{2+}]_i$ oscillations is accompanied by a disruption of glucose sensitivity and impairment of the normal oscillatory pattern of insulin secretion.

2 AIMS

The overall objective of this thesis was to investigate the metabolic consequences of SNAP-25b-deficiency in order to better understand the role of the two splice variants, SNAP-25a and SNAP-25b. The specific aims investigated have been to study:

- If the replacement of SNAP-25b with SNAP-25a (*i.e.* a small modification in the SNARE complex) could provoke metabolic abnormalities in mice, alone or in combination with a high fat/high sucrose diet consumption.

- The effects of SNAP-25b-deficiency on islet physiology and glucose-stimulated insulin secretion.

- The binding capabilities of the SNAP-25 isoforms for proteins regulating initiation and inhibition of membrane fusion.

3 MATERIALS AND METHODS

All the experiments were carried out in different cohorts of mice and each of them included the following groups of 12-week-old mice depending on the paper: SNAP-25b-deficient (MT) and wild type (WT) littermates, males and females fed a control (CoD) or high fat/high sucrose (Western, WeD) diet.

3.1 *IN VIVO* EXPERIMENTS

3.1.1 Animals

The SNAP-25b-deficient mice were generated as previously described [52]. The animals were maintained on a regular dark-light cycle (lights on at 07:00 and off at 19:00) in temperature and humidity-controlled rooms with food pellets and tap water *ad libitum*. MT and WT littermates were euthanised by cervical dislocation. Animal studies were done in accordance with the guidelines from the local authorities, *i.e.*, the Stockholm Northern Animal Experiments Ethics Board, following the approval of the Administration of the Republic of Slovenia for Food Safety, Veterinary Sector and Plant Protection (Permit number: 34401-61-2009/2, 34401-46/2014/4, 34401-12/2015/3) and in accordance with Directive 2010/63/EU of the European parliament and of the Council on the Protection of Animals Used for Scientific Purposes.

3.1.2 Diet

The diet intervention started at the age of 5 weeks, *i.e.*, at adolescence, a critical window for the development of metabolic disorders [104]. MT and WT mice from each sex were divided randomly into two groups with a similar average body weight and were fed either CoD (10.5% of kilocalories from fat, 17.7% from proteins; and 71.7% from carbohydrates) or the WeD (40.0% of kilocalories from fat; 17.0% from proteins; and 43.0% from carbohydrates) for 7 weeks. In Paper I mice were either fed a CoD or WeD, whereas in Paper I and II only a CoD.

3.1.3 Measurement of metabolic parameters

In Paper I, the mice were housed three per cage, and body weight was monitored for each genotype and sex twice a week during the whole time course of the diet intervention. At the end of the study, the BMI was calculated. Nonfasting blood glucose was determined once a week during the 7 weeks of diet intervention in blood obtained from the tail vein at the start of the dark cycle (7:00 PM) with a FreeStyle Glucometer (Abbott Diabetes Care, Witney, United Kingdom). Preprandial blood triglycerides and cholesterol levels were determined

using a multiparameter diagnostic device for triglycerides and cholesterol (multiCare-in, Biochemical Systems International, Florence, Italy) from the tail vein. At the end of the diet-intervention study, this cohort of animals was subjected to 12 h overnight starvation, and then basal blood triglycerides and cholesterol levels were determined.

3.1.4 Feeding pattern and caloric intake

In Paper I, mice were placed in individual cages and food intake was determined twice a week. Because the calorie intake differed between the two diets, daily calorie consumption was calculated as the kilocalories ingested daily by each mouse. Finally, calorie efficiency was determined to establish the relationship between body weight gain and calories consumed by each animal (Δ body weight/kcal). All these parameters were corrected for the body weight of each individual animal in each experimental group. The male MT mice fed a CoD became overweight, despite that their average food intake was significantly lower than WTs. Thus, we monitored their daily food intake, body weight, and body weight gain at 7:00 AM (after the active period) and at 7:00 PM (after the inactive period).

3.1.5 Glucose tolerance tests and serum insulin levels

In Paper I, mice were starved 12 h overnight and the basal blood glucose (0 time point) was measured in blood samples collected from the tail vein. Thereafter, mice received an intraperitoneal glucose injection (2 g/kg body weight), and blood glucose was measured after 15, 30, 60, 90, and 120 min. Blood glucose levels were determined using a FreeStyle Glucometer (Abbott Diabetes Care, Witney, United Kingdom). Blood was collected at the same time points as in the glucose tolerance test (GTT), centrifuged for 20 min, 10,000 x g at 4 °C and serum was frozen at -80 °C until use. Serum insulin levels were analysed using an ultrasensitive mouse insulin ELISA kit (Crystal Chem Inc., Downers Grove, IL, USA). The $HOMA_{IR}$ was calculated using the formula: fasting insulin (mU/L) × fasting blood glucose (mmol/L)/22.5. The AUC was calculated using the basal levels of blood glucose and serum insulin as baselines.

In Paper II, a "first phase" GTT was performed on mice starved 12 h overnight. One hour before glucose injection, EMLA cream (25 mg lidocaine and 25mg prilocaine, AstraZeneca, London, United Kingdom) was applied on the tail (to minimise stress) and after 15 min basal blood glucose was measured. After 45 min mice were injected intraperitoneally with glucose (2g/kg body weight) and blood glucose levels were determined at 0, 2.5, 5, 7.5, 10, 15 min. Serum insulin, $HOMA_{IR}$ and AUC were measured as in Paper I.

3.2 *EX VIVO* EXPERIMENTS

3.2.1 Total pancreas insulin content

The whole pancreas was dissected out and homogenised in 1.4 ml of acid ethanol containing 75% (v/v) ethanol in 0.2 M HCl until no big pieces were observed. The pancreas homogenates were sonicated (frequency: 30 Hz; 12 pulses) (Branson Sonifier Cell Disruptor B15; Branson Ultrasonic, Danbury, CT, USA) and diluted at 1:5,000, 1:10,000, and 1:20,000 for insulin measurement with an ultrasensitive mouse insulin ELISA kit (Crystal Chem Inc., Downers Grove, IL, USA). Protein levels in each pancreas homogenate were measured by the Bradford method, and the total pancreas insulin content (ng/ml) obtained from ELISA immunoassay was normalised to the total protein concentration (mg/ml) of each extract.

3.2.2 Body fat distribution

Subcutaneous (ScAT) and visceral (mesenteric, MsAT, retroperitoneal, RpAT and perigonadal PgAT) white adipose tissues were dissected out quickly and weighted. Afterwards, they were frozen in liquid nitrogen and kept at −80 °C until use.

3.2.3 Leptin and ghrelin in serum

For leptin and ghrelin measurements, multiplex immunoassays (BioPlex Pro, Bio-Rad Laboratories, Hercules, CA, USA) were run with blood samples taken randomly from animals belonging to the different cohorts, always after a 12 h period of overnight starvation.

3.2.4 Triglycerides content in liver

The left lobe of each liver (100-300 mg) was dissected out, immersed quickly in 350 µl of ethanolic KOH [0.1 M potassium hydroxide (Sigma-Aldrich, ST. Louis, MO, USA) in absolute ethanol (Merck, Darmstadt, Germany)], and incubated overnight at 55 °C until no oil layer was visible. After homogenization, each sample was brought up to 1 ml with a 1:1 ethanol:water solution, vortexed, and centrifuged at 4 °C (7,000 × *g*) for 5 min. The supernatant was moved to another tube, and again the volume was brought up to 1.2 ml with a 50% (v/v) ethanol solution. 200 µl of each sample were neutralised with 215 µl of 1 M $MgCl_2$ solution, vortexed, and left on ice for 10 min. After incubation, samples were centrifuged under the conditions described above, and the supernatant was moved to a new tube. Free liver triglycerides were analysed using Free Glycerol Reagent and Glycerol Standards (Sigma-Aldrich, ST. Louis, MO, USA) to construct the standard curve. The glycerol concentration in each cuvette (triolein equivalents) was measured by spectrophotometry (SAFAS-MONACO spectrophotometer, Monaco, France) at a wavelength

of 540 nm and was determined by extrapolation with the standard curve. Total triglycerides content expressed in milligrams per gram of liver was calculated.

3.2.5 Isolation and cultivation of islets of Langerhans

After sacrifice, abdomen was accessed via laparotomy and collagenase P (1 mg/ml) (Roche, Mannheim, German) diluted in HBSS pH 7.4 (Thermo Scientific, Waltham, MA) was injected into the proximal common bile duct clamped distally at the major duodenal papilla of Vater. After injection, the pancreas was extracted and incubated in HBSS at 37 °C for 30 min without shaking. Ice-cold HBSS (without BSA) was added and 1-2 strokes with 18G needle was applied to dislodge islets attached to the tissue. After 4 washes (2 with HBSS without BSA and 2 with HBSS 0.5% BSA) islets were hand-picked under a stereo microscope (KL200 LED, Leica, Wetzlar, Germany). Purified islets were transferred into petri dishes containing RPMI-1640 (Thermo Scientific, Waltham, MA, USA) with a final concentration of heat inactivated foetal bovine serum (10%), glutamine (2 mM), penicillin (100 U/ml) and streptomycin (100 µg/ml) (Thermo Scientific, Waltham, MA, USA) and incubated at CO_2 (5%) and 37 °C overnight.

3.2.6 Dynamic insulin secretion assay

After overnight incubation, approximately 80 islets from each pancreas were transferred to a chromatograph column (PERI-4.2, BioRep technologies, Miami Lakes, FL, USA) filled with Bio-Gel P-4 (Bio-Rad Laboratories, Hercules, CA, USA) to stabilise them during the perifusion. Islets were pre-perifused with NaCl (125 mM), KCl (5.9 mM), $CaCl_2$ (1.28 mM), $MgCl_2$ (1.2 mM), HEPES (25 mM), BSA (0.1%) and glucose (3 mM), pH 7.4 for 45 min at 37 °C. The islets were perifused in the buffer above for 12 min, then sequentially exposed to 11 mM glucose for 35 min followed by 3 mM glucose for 15 min and the protocol finished with 25 mM KCl + 3 mM glucose for 15 min to fuse all possible insulin granules. Fractions (50 µl) of the perifusates were collected every min during stimulation in a 96-well plate. The collected fractions were then measured for insulin concentration by the AlphaLISA detection kit (PerkinElmer, Waltham, MA, USA) with a plate reader (EnVision2103, PerkinElmer, Waltham, MA, USA).

3.3 HISTOLOGY AND IMMUNOHYSTOCHEMISTRY

3.3.1 Adipocyte size quantification

After dissection, ScAT and PgAT tissues were formalin-fixed by immersion for 2 weeks. After fixation, both ScAT and PgAT were placed in 10% (v/v) sucrose-impregnated cardboard blocks, frozen in dry ice, and stored at −80 °C until use. Tissues were sectioned at

20-µm thickness using a cryostat (Microm HM500M/CryoStar NX70, Thermo Scientific, Waltham, MA, USA) and thawed onto SuperFrost Plus microscope slides (VWR International, Radnor, PA, USA). Slides were stained with H&E (Histolab, Gothenburg, Sweden) and mounted in VectaMount permanent mounting medium (Vector Laboratories, Inc., Burlingame, CA, USA). The stained adipocytes were analysed in an optical microscope (Leica, Wetzlar, Germany), and images were obtained at 10× and 40× magnification objectives. The area of the adipocytes (in square micrometres) was analysed using the ImageJ program (National Institutes of Health, Bethesda, MD, USA), and images were obtained with the 10× magnification objective.

3.3.2 Oil red "O" staining in liver

For lipid visualization, oil red "O" (ORO) staining was conducted on 14-µm-thick liver sections. Before sectioning, liver samples from the left lobe of each animal were dissected out and formalin-fixed for 24 h. Sections were obtained as in 3.3.1. After 1 h at room temperature slides were rinsed in 60% (v/v) isopropyl alcohol, stained in freshly prepared 0.1% ORO solution (Sigma-Aldrich, ST. Louis, MO, USA) for 15 min, rinsed in 60% (v/v) isopropyl alcohol, washed in distilled water, and mounted with 0.25% DABCO mounting medium (Sigma-Aldrich, ST. Louis, MO, USA). Liver sections from all experimental groups were analysed, and lipid droplets were identified using a 5× objective (Leica) followed by amplification to 10× and 40× magnification.

3.3.3 Analysis of islets parameters

For histological and immunohistochemical analysis, the animals were perfused and the pancreas treated as described in 3.3.4. Thaw-mounted 16 µm sections were dried at room temperature for 30 min and rinsed with PBS for 15 min. Mounted sections were incubated with primary antibodies in a humidified chamber at 4 °C overnight (rabbit anti-glucagon antibody, 1:1,000 dilution, BioGenex, Fremont, CA, USA and guinea-pig anti-insulin antibody, 1:200 dilution, Bio-Yeda, Rehovot, Israel). After washing in PBS, they were incubated with secondary antibodies for 90 min at room temperature (donkey Cy3-conjugated anti-rabbit IgG and donkey FITC-conjugated anti-guinea pig IgG, 1:150 and 1:40 dilution respectively, Jackson Immunoresearch Europe, Suffolk, United Kingdom). Sections were finally incubated with DAPI (1:10,000 dilution, Bio-Rad, Hercules, CA, USA) diluted in PBS for 15 min at room temperature and mounted using 2.5% DABCO in glycerol (Sigma-Aldrich, ST. Louis, MO, USA). For the detection of apoptotic beta cells, sections were processed according to the instructions in the commercial kit used (Click-iT Plus TUNEL assay, Thermo Scientific, Waltham, MA) and co-labeled with insulin. For histology, another

set of sections was used for H&E staining (Histolab, Gothenburg, Sweden) and mounted with VectaMount permanent mounting medium (Vector Laboratories Inc., Burlingame, CA, USA).

The pancreatic sections were examined with Nikon Eclipse E600 fluorescence microscope with objective lenses 20× (Nikon, Tokyo, Japan) equipped with appropriate filters and ORCA-ER, C4742-80 digital camera (Hamamatsu Photonics K.K., Shizuoka, Japan), using Hamamatsu Photonics Wasabi 150 software. Images were also acquired by use of upright laser scanning confocal microscope based on a Leica TCS-SP5 II (Leica Microsystems, Wetzlar, Germany), together with long-distance water-dipping objectives (Leica HXC-APO 20×/0.5, Wetzlar, Germany), and a Leica LAS software (Leica, Wetzlar, Germany). For insulin- and glucagon-expressing cell quantifications, one randomly-chosen pancreatic section/animal was used, each insulin/glucagon positive cell with detectable nucleus was counted and the number of cells was divided by the islet area. Two randomly-chosen H&E stained pancreatic sections/animal were used for islet size measurement and number of islet per section. Around 400 islets were counted. All measurements were done with the ImageJ program (National Institutes of Health, Bethesda, MD, USA). For the detection of apoptotic beta cells, one randomly-chosen pancreatic section/animal was used and all islets within a section were analysed.

3.3.4 Proximity ligation assay

For histological and immunohistochemical analyses, mice were deeply anesthetised with isofluorane and transcardially perfused with 20 ml of warm (37 °C) PBS, pH 7.4, followed by 20 ml of a warm mixture of 4% paraformaldehyde (37 °C) and 0.4% picric acid in 0.16 M phosphate buffer (pH 7.2), and then by 50 ml of the same, but ice-cold fixative. The pancreas was dissected out and postfixed in the same fixative for 90 min at 4 °C. Specimens were subsequently stored in 10% sucrose in PBS (0.1 M, pH 7.4) containing 0.01% sodium azide (Sigma, St. Louis, MO, USA) and 0.02% bacitracin (Sigma) as preservatives at 4 °C for 2 days. Coronal sections (14 μm thick) were cut as described in 3.3.1. Afterwards, they underwent the protocol for proximity ligation assay (PLA) (DuoLink in situ bright-field, Sigma-Adrich, MO, USA). Primary antibodies against Gβ1-4 (1:150 dilution, M-14, Santa Cruz Biotechnology, Dallas, TX, USA) and SNAP-25 (1:1,000 dilution, SMI-81, Biolegend, San Diego, CA, USA) were used.

3.4 PROTEIN ANALYSES

3.4.1 Western blotting in hypothalamus and liver

In Paper I, hypothalamus and liver samples from all experimental groups were homogenised in ice-cold buffer containing 0.42 mM NaCl, 20 mM Hepes (pH 7.9), 1 mM $Na_4P_2O_7$, 1 mM EDTA, 1 mM EGTA, 1 mM DTT, 20% (v/v) glycerol, 1 μg/ml aprotinin, 1 μg/ml leupeptin, 20 mM sodium fluoride, 1 mM trisodium orthovanadate, and 2 mM phenylmethylsulfonyl fluoride. Tubes containing homogenates were exposed to a thermal shock at −80 °C in liquid nitrogen and thawed to 37 °C three consecutive times, and centrifuged at 10,000 × g for 20 min. Then the supernatant was collected. Protein levels in the supernatant of both liver and hypothalamus homogenates were measured by the Bradford method, and volumes were adjusted in Laemmli buffer [50 mM Tris (pH 6.8), 10% (v/v) SDS, 10% (v/v) glycerol, 5% (v/v) mercaptoethanol, and 2 mg/ml bromophenol blue] to 2 μg/μl of protein concentration. Proteins (40 μg) were loaded using a Trans-Blot apparatus (Bio-Rad). Each sample was size-separated in 10% (v/v) SDS/PAGE and transferred to PVDF membranes (GE Healthcare, Little Chalfont, United Kingdom). For immunoblotting, membranes were blocked with 5% (w/v) nonfat dried milk. Primary antibodies against total and phosphorylated (Thr^{172}) forms of AMPK-$\alpha_{1/2}$ (1:1,000 dilution, Cell Signaling, Danvers, MA, USA), total and phosphorylated (Tyr^{705}) STAT3 (1:1,000 dilution, Santa Cruz Biotechnology, Dallas, TX, USA), total and phosphorylated (Thr^{202}/Tyr^{204}) ERK1/2 (1:1,000 dilution, Cell Signaling, Danvers, MA, USA), or ObR (1:1,000 dilution, Santa Cruz Biotechnology, Dallas, TX, USA) were applied overnight. After incubation with IgG–peroxidase complexes, blots were incubated in commercial enhanced chemiluminescence reagents (ECL-Prime; GE Healthcare, Little Chalfont, United Kingdom), and membranes were exposed to a luminescent image analyser (Las-1000 Plus; Fuji, Tokyo, Japan). Obtained images were quantified using ImageJ software. Values for all proteins were normalised to β-actin (1:1,000 dilution, Sigma-Aldrich, ST. Louis, MO, USA).

3.4.2 Western blotting and immunoprecipitation in hippocampus

In Paper III, hippocampi were quickly dissected and homogenised in ice-cold buffer containing: 50 mM Tris-HCl (pH 7.4), 180 mM NaCl, 0.25% NP-40, 20% glycerol, 1 mM $MgCl_2$, 2 mM EDTA, 0.035% β-Mercaptoethanol, 0.5 mM phenylmethanesulfonylfluoride and proteases inhibitor cocktail (1 tablet/10ml; Roche, Basel, Switzerland) by using Kontes pellet pestle homogeniser (Sigma-Aldrich, St. Louis, MO, USA). Protein concentration was assessed as in 3.4.1 and adjusted with the lysis buffer to a final concentration of 2 μg/μl. One ml of precleared protein extracts was incubated overnight at 4 °C under rotation with 50 μl of

protein G-sepharose slurry (GE Healthcare, Little Chalfont, United Kingdom) preincubated with 1 µg of anti-SNAP-25 antibody (SMI-81, Biolegend, San Diego, CA, USA) diluted in 50 µl of TBS buffer (50 mM Tris-HCl, pH 7.4, 150 mM NaCl). After four washes with TBS buffer supplemented with 0.05% Triton X-100, 25µl of Laeammli buffer was added to the precipitated proteins (0.5 M Tris-HCl pH 6.8, 20% glycerol, 4% SDS, 10% β-Mercaptoethanol and 0.05% bromophenol blue) and heated at 100 °C for 20 minutes. Protein eluates were centrifuged 3 min at 6000 rpm and 15 µl were loaded on 4-12% Bis-Tris gradient gels (NuPage, Thermo Fisher Scientific, Waltham, MA, USA) and run for 45 min at 200 V with 2-(N-morpholino)ethanesulfonic acid (MES) buffer (NuPage, Thermo Fisher Scientific, Waltham, MA, USA). For silver staining the gels were processed as described in the protocol (SilverQuest™ Silver Staining Kit, Thermo Fisher Scientific, Waltham, MA, USA). Proteins were transferred onto nitrocellulose membranes by using the iBlot gel transfer technique (Thermo Fisher Scientific, Waltham, MA, USA). For immunoblotting, membranes were blocked with 5% nonfat dried milk in 0.1% Tween-PBS (4.3 mM Na_2HPO_4, 137 mM NaCl, 2.7 mM KCl and 1.4 mM KH_2PO_4, pH 7.4) for 2 h at room temperature. Primary antibodies against syntaxin 1 (1:500,000 dilution, Synaptic Systems, Göttingen, Germany), VAMP-2 (1:1,000,000 dilution, Synaptic Systems, Göttingen, Germany) Munc18-1 (1:10,000 dilution, Synaptic Systems, Göttingen, Germany) Gβ1-4 (1:500 dilution, M-14, Santa Cruz Biotechnology, Dallas, TX, USA), and SNAP-25 (1:1,000,000 dilution, SMI-81, Biolegend, San Diego, CA, USA), were applied overnight at 4 °C under shaking. After incubation with anti-mouse or anti-rabbit IgG-peroxidase complexes (GE Healthcare, Little Chalfont, United Kingdom), immunoreactive bands were processed as described in 3.4.1. Values for Gβ1-4 band densitometry were normalised to SNAP-25 band densitometry.

For analysing expression levels of hippocampal proteins, 15 µg of protein from lysates were loaded and run on gradient gels with the same materials and conditions as for the immunoprecipitation described above. Primary antibodies against Munc18-1 (1:10,000), syntaxin 1 (1:100,000), VAMP-2 (1:1,000,000), SNAP-25 (1:1,000,000) and Gβ1-4 (1:5,000) and α-tubulin (1:1,000 dilution, Santa Cruz Biotechnology, Dallas, TX, USA) were used. Values for the proteins band densitometry were normalised to α-tubulin.

3.4.3 Mass spectrometry

Samples were analysed at Proteomics Karolinska, PK/KI core facility at Karolinska Institutet, Stockholm, Sweden. The silver-stained protein band was cut from the gel and the piece was digested using MassPREP robotic protein handling system (Waters, Millford, MA, USA). Briefly, washing was carried out in 50 mM ammonium bicarbonate containing 50%

acetonitrile. The protein was reduced (DTT) and alkylated (iodoacetamide) followed by in-gel digestion with 0.3 mg trypsin (Promega, Madison, WI, USA) in 50 mM ammonium bicarbonate for 5 h at 40 °C. The tryptic peptides were extracted with 1% formic acid/2% acetonitrile, followed by 50% acetonitrile twice. The liquid was evaporated and the peptides were injected onto the LC-MS/MS system (EASY-nLC chromatography system and Orbitrap Velos Pro API mass spectrometer, Thermo Scientific, MA, USA). The peptides were separated on a homemade C18 column, 8 cm (Silica Tip 360 µm OD, 75µm ID, New Objective, Woburn, MA, USA) and the effluent electrosprayed into the mass spectrometer direct via the column. The spectra were analysed using Mascot (Matrix Science) and searched against SwissProt_2014_01, mus musculus.

3.5 ELECTROPHYSIOLOGY AND CA^{2+} IMAGING IN BETA CELLS

3.5.1 Pancreatic tissue slice preparation

A low-melting point agarose (1.9 %, Lonza Rockland Inc., Rockland, ME, USA) in extracellular solution, ECS, consisting of: NaCl (125 mM), $NaHCO_3$ (26 mM), glucose (6 mM), lactic acid (6 mM), myo-inositol (3 mM), KCl (2.5 mM), Na-pyruvate (2 mM), $CaCl_2$ (2 mM), NaH_2PO_4 (1.25 mM), $MgCl_2$ (1 mM), ascorbic acid (0.5 mM) at 40 °C was injected into the proximal common bile duct clamped distally at the major duodenal papilla of Vater. Immediately thereafter, the pancreas was cooled using ice-cold ECS and extracted. Small tissue blocks were plunged into the agarose at 40 °C and cut with a VT 1000 S vibratome (Leica, Nussloch, Germany) into 140 µm-thick slices of a surface area of 20-100 mm^2. Throughout the procedure, tissue was held in an ice-cold ECS continuously bubbled with a gas mixture containing O_2 (95%) and CO_2 (5%) at barometric pressure to ensure oxygenation and a pH of 7.4. After cutting the slices were collected in 30 ml of HEPES-buffered saline, HBS, consisting of: NaCl (150 mM), HEPES (10 mM), glucose (6 mM), KCl (5 mM), $CaCl_2$ (2 mM), $MgCl_2$ (1 mM); titrated to pH 7.4. All chemicals were obtained from Sigma-Aldrich (St. Louis, MO, USA) unless indicated.

3.5.2 Electrophysiology

Patch pipettes were pulled from borosilicate glass capillaries (GC150F-15, Harvard Apparatus, Holliston, MA, USA) using a horizontal pipette puller (P-97, Sutter Instruments, Novato, CA, USA). The pipette resistance was 2–3 MΩ in Cs^+-based solution. Fast pipette capacitance (C_{fast}) was compensated in cell-attached mode, slow membrane capacitance (C_{slow}) and series conductance (Gs) were compensated after establishment of whole-cell mode. Only experiments with Gs>50 nS were carried out. Recordings were performed in the

standard whole-cell mode via a patch-clamp lock-in amplifier (SWAM IIc, Celica, Slovenia) connected to a computer via A/D converter (16 bit, NI USB-6343, X Series Multifunction DAQ, National Instruments, Austin, TX, USA) and recorded on the hard disk using WinWCP V5.1.6 software (John Dempster, University of Strathclyde, United Kingdom). The same software was used for identifying beta cells by their Na^+ current inactivation properties and for determining membrane capacitance change after slow photo-release of caged Ca^{2+}. A continuous sine voltage (1600 Hz, 11 mV RMS amplitude) was applied to measure C_m. Resting membrane potential in voltage-clamp mode was -80 mV. The pipette solution used for Ca^{2+}-induced capacitance and current measurements was composed of NP-EGTA (5 mM), $CaCl_2$ (4 mM), mM Fura 6F (0.1) (Invitrogen, Eugene, OR) together with CsCl (125 mM), HEPES (40 mM), $MgCl_2$ (2 mM), TEA–Cl (20 mM), Na_2ATP (2 mM) at pH 7.2 and osmolality 300 ± 10 mOsm. Signal processing and curve fitting was done using Matview (Wise Technologies, Ljubljana, Slovenia) and Matlab (The MathWorks, Inc., Natick, MA, USA).

3.5.3 Loading of dyes and imaging of $[Ca^{2+}]_i$ oscillations in beta cells

For $[Ca^{2+}]_i$ imaging 8-10 slices were incubated in a petri dish filled with HBS (3.333 ml) containing Oregon Green 488 BAPTA-1 acetoxymethyl ester calcium fluorescent dye (6 μM, OGB-1, Invitrogen, Eugene, OR, USA), Pluronic F-127 (0.03 % w/v) and dimethylsulphoxide (DMSO, 0.12% v/v) for 50 min on an orbital shaker (50 turns min^{-1}) at room temperature and protected from light. Ca^{2+} imaging was performed on a Leica TCS SP5 AOBS Tandem II upright confocal system using a Leica HCX APO L 20× water immersion objective (NA = 1.0). OGB-1 was excited by an argon 488 nm laser and the emitted light was detected by Leica HyD hybrid detector in the range of 500-700 nm (all from Leica Microsystems GmbH, Wetzlar, Germany). The slices were perifused with bubbled ECS at 35-37 °C containing 6-12-6 mM glucose, sequentially. Only cells lying at least 15 μm below the surface were imaged. Images were acquired at a spatial resolution of 512 × 512 pixels and a temporal resolution of 1 Hz. The total time of 12 mM glucose stimulation was 15-22 min. To determine the frequencies and the durations of Ca^{2+} oscillations and for the network analysis, images were acquired for 5 min at a spatial resolution of 256 × 256 pixels and a temporal resolution of 29 Hz. Time traces were analysed off-line from regions of interest with Leica Application Suite Advanced Fluorescence software (Leica Microsystems GmbH, Wetzlar, Germany), exported and further examined to determine the delays in the onsets and delays in deactivation in the $[Ca^{2+}]_i$ responses using MATLAB (The MathWorks, Inc., Natick, MA, USA). Traces were corrected for photobleaching of the dye employing a

combination of linear and single exponential fit [90]. Signals were expressed as (F – F0)/F0 ratios, where F0 is the initial fluorescence intensity and F is the fluorescence signal recorded at an individual time point. All recorded time series were digitally band-pass filtered in order to remove noise and artefacts, and then additionally smoothed with an adjacency averaging procedure. To calculate the frequencies and durations of Ca^{2+} oscillations, the onsets and the endings of individual oscillations were defined as the time in which the signal decreases bellow the half of the maximal amplitude in the given oscillation. In this manner, the activity profiles of all cells were binarized, whereby the time between the onset and ending of an oscillation was denoted as 1, whilst 0 otherwise. The cells with a low signal-to-noise ratio were excluded from further analyses.

3.5.4 Synchronization and functional connectivity of beta cells

The level of synchronization among beta cells was determined on the basis of binarised Ca^{2+} activity by means of the coactivity matrix, whose *ij*-th element is defined as follows:

$$Cij = \frac{Tij}{\sqrt{TiTj}}$$

and reflects synchronization between the *i*-th and the *j*-th cell. In the equation, Tij stands for the total coactivity time in which both cells were simultaneously active and Ti and Tj are the total individual activity times for both cells. If $Cij = 0$ then no correlation between the *i*-th and *j*-th cells exists, whilst $Cij = 1$ signifies completely synchronous and aligned dynamics. To describe the global level of synchronization in the whole slice, the mean coactivity was calculated by averaging over all cell pairs (Figure 5).

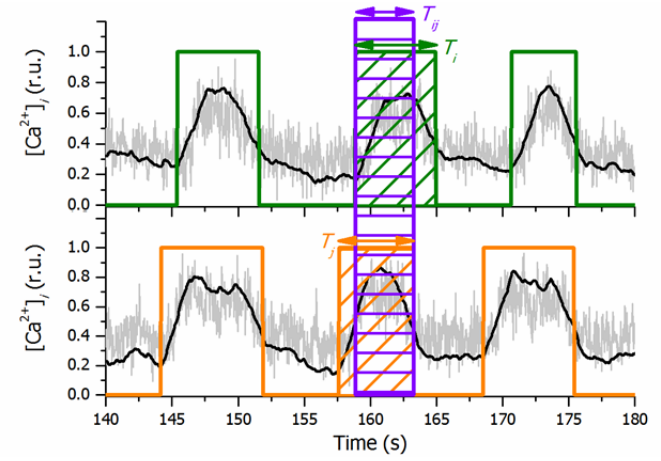

Figure 5. Quantification of the Ca^{2+} traces in beta cells. The grey lines represent the recorded Ca^{2+} traces of two active beta cells upon glucose stimulation. The black lines represent the traces after removal of noise and smoothening. Traces were then binarised. The level of synchronization among beta cells was calculated as the coactivity coefficient, which measures the overlap of activity (T*ij*, violet area) of *i*-th (T*i*, green area) and *j*-th (T*j*, orange area). Supplementary figure from Paper II.

To get a more detailed insight into the intercellular interaction patterns, functional connectivity maps were constructed. Two cells were considered to be functionally connected if their activity profiles showed a high enough degree of synchronization, *i.e. Cij* exceeded a given threshold value. A variable connectivity threshold was used in order to ensure that all examined beta cell networks had the same mean number of connections per cell – 6. The segregation of beta cell networks was assessed by calculating a global metric called "modularity", as proposed by Blondel *et.al.* [105]. A higher modularity indicated a high degree of sub-compartmentalization, whereas close-to-zero values indicated an integrated and a module-free network.

3.6 STATISTICAL ANALYSES

In Paper I, StatView 5.0 software was used for statistical analyses. Cell-line charts were analysed by repeated-measures ANOVA. For time point by time point analysis, two-way ANOVA was used. Cell bar charts were analysed by two-way ANOVA. Unpaired *t*-test analysis was used to compare one experimental group with its corresponding control group during physiological conditions. Statistical significance was verified with nonparametric statistics using the Kruskal–Wallis H-test, followed by the post hoc Mann–Whitney, Fisher's protected least significant difference, and Student–Newman–Keuls tests. Bonferroni correction was applied in all statistical analyses. The variance between groups was tested using Bartlett's test and was examined in all datasets. Normal distribution was verified by using the Kolmogorov–Smirnov normality test.

In Paper II and III, all statistical analyses were done using GraphPad Prism (GraphPad Software, San Diego, CA, USA). Two-way ANOVA followed by Bonferroni multiple comparisons test, Mann-Whitney and Student´s *t*-test were used to verify statistically significant differences in all our experiments dependently on non-Gaussian or Gaussian distribution of data. The level of significance was set at a P value < 0.05.

3.7 SCHEMATIC METHODOLOGICAL APPROACH

The schematic methodological approach for each study is illustrated in Figure 6 (Paper I), Figure 7 (Paper II) and Figure 8 (Paper III).

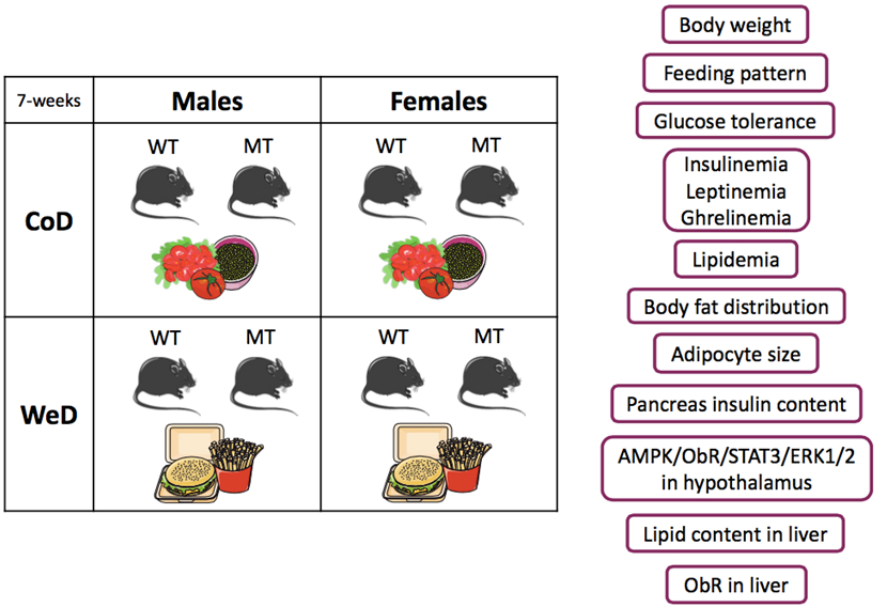

Figure 6. Methodological approach in Paper I.

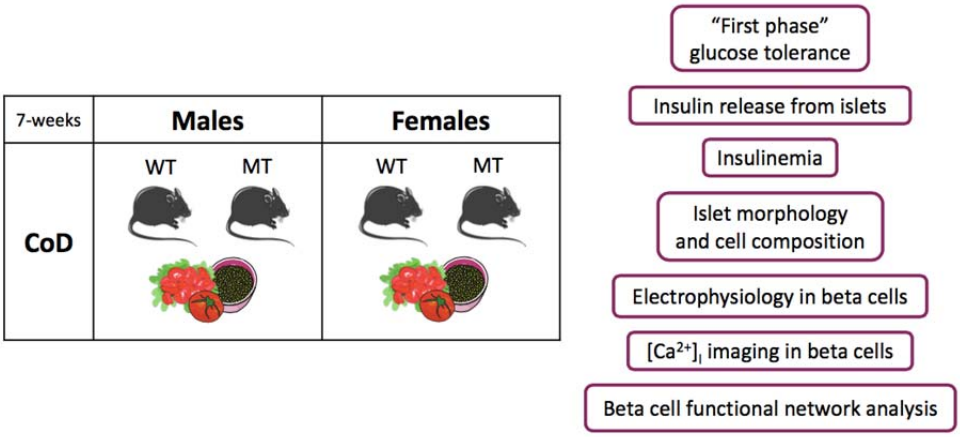

Figure 7. Methodological approach in Paper II.

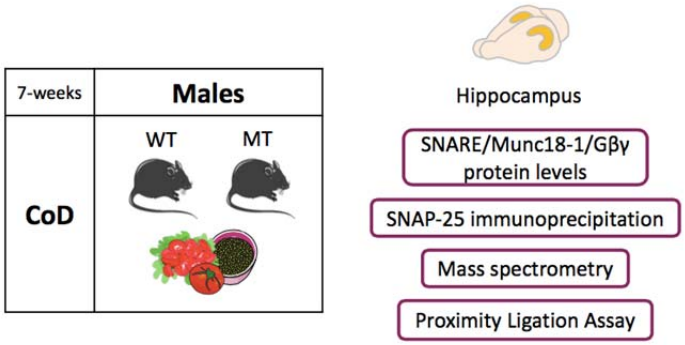

Figure 8. Methodological approach in Paper III.

4 RESULTS AND DISCUSSION

4.1 PAPER I

Deregulation of hormonal secretion, such as insulin, is regarded as a secondary sign and consequence of developing metabolic syndrome [8]. In Paper I, we instead explored if a small modification in the exocytosis machinery could provoke metabolic syndrome, therefore acting as a genetic predisposition. We took advantage of MT mice which express SNARE complexes only formed by SNAP-25a in neuronal, neuroendocrine and endocrine cells [52]. Little is known about the functional difference between SNAP-25a and SNAP-25b, yet SNAP-25a was found to have a lower capacity to keep vesicles in a primed state [42]. We monitored WT and MT mice for 7 weeks from the age of 5 weeks. We started the diet intervention during adolescence since it is a critical window for the development of metabolic syndrome [104,106]. Both male and female mice were either administered a CoD or a WeD. We found that SNAP-25b-deficiency provoked a set of symptoms characteristic of the human metabolic syndrome, exacerbated when combined with WeD. Interestingly, a number of polymorphisms in genes encoding proteins important for insulin exocytosis (including SNAP-25) have been linked to the severity of certain metabolic traits in T2D/obese patients or susceptibility for T2D [107–111]. It is therefore tempting to speculate that in humans such mutations, in combination with hypercaloric diets, can contribute to the initial phase of development of metabolic syndrome.

4.1.1 SNAP-25b-deficient mice develop obesity and impaired insulin and glucose homeostasis

At the beginning of the study, at the fifth postnatal week, WT and MT mice showed similar body weights and blood glucose/triglycerides/cholesterol levels. During the intervention, we noticed that MT mice fed a CoD had significantly higher body weights compared to WTs. The body weight gain in WeD-fed WTs was similar to the CoD-fed MTs, whereas WeD-fed MT mice dramatically increased their body weights compared to all other experimental groups. We monitored insulin and glucose homeostasis by challenging 11-week-old mice with a standard GTT and concomitant collection of serum from the tail vein to analyse insulin levels. Already at basal conditions, all groups of females demonstrated a significant increase in basal blood glucose compared to CoD-fed WTs, whereas in males the effect was significant only in WeD-fed MTs. The basal insulin levels were increased in all groups compared to CoD-fed WTs but only in males WeD-fed MTs it was statistically significant. When challenged with glucose, both male and female MTs on CoD exhibited significantly lower blood glucose levels compared to WTs after 15 min which was accompanied by

elevated serum insulin levels. This suggested that the presence of SNAP-25a alone can favour insulin exocytosis at a lower stimulatory threshold. When the animals were fed a WeD the glucose clearance was dramatically impaired. Moreover, we found increased total pancreas insulin content in MT mice. By monitoring preprandial blood glucose levels for 7 weeks of diet intervention, we found that MT mice developed hyperglycaemia compared to CoD-fed WT mice. We could disclose both genetic and diet influences in the development of hyperglycaemia in males and females. The inability of maintaining normal blood glucose suggested insulin resistance and/or impaired eating habits. Indeed, the $HOMA_{IR}$ revealed only a tendency to insulin resistance in males but a robust effect in MT-CoD females compared to WT-CoD.

4.1.2 SNAP-25b-deficient mice display altered eating habits correlated to hypothalamic dysfunctions

To explain the increased body weight in MT-CoD as well as MT-WeD mice, we investigated their eating habits. In males, the average food and calorie intake of the CoD-fed MTs was significantly lower than that of the CoD-fed WTs whereas in the MT females the result was opposite, partially explaining their body weight gain. Monitoring the male CoD-mice every day for 7 days, enabled us to find that in WTs, the calorie intake was mainly associated with the dark active period whereas in MTs it was equally distributed during both the light and dark period, suggesting a disruption of the circadian feeding behaviour.

We therefore hypothesised that the lack of SNAP-25b could induce alterations in feeding circuits in hypothalamic neurons hence influencing the mouse metabolic homeostasis [3,112]. A hallmark for metabolic dysfunction is the activation/phosphorylation of a master metabolic regulator, AMPK, regarded as a key protein in the leptin signalling pathway [113,114]. The activation status of AMPK-$\alpha_{1/2}$ subunit in the hypothalamus after 7 weeks of diet intervention was compromised in a sex-independent manner in all groups when compared to CoD-fed WTs. We further investigated the status of the leptin receptor, ObR, since it is well described that genetic and diet-induced obesity account for increased leptin levels and consequent leptin resistance in a tissue specific manner [115]. In hypothalamus, the long isoform of ObR, ObRb, was found to be affected by WeD intervention in a similar manner in WTs and MTs in both sexes, but with the MTs having the most dramatic ObRb deficiency. We further characterised the expression levels of key proteins in the insulin/leptin signalling pathways such as STAT3 and ERK1/2. The phosphorylated STAT3 was reduced in all groups compared to CoD-fed WTs, except for male CoD-fed MT mice. The phosphorylated form of ERK1/2 was increased in all experimental groups, a phenomenon described as a low-grade inflammation in the

hypothalamus of individuals with obesity and T2D [116]. Taken together, our results suggest that the effects of SNAP-25b-deficiency in combination with WeD are accompanied by disruption of cross-talk between the brain (in particular the hypothalamus) and the periphery. These results are in line with work from other groups where diet-induced obesity and insulin resistance induce permanent effects both on the periphery and the brain.

4.1.3 SNAP-25b-deficiency leads to adiposity accumulation and dyslipidaemia

As SNAP-25b-deficiency alone provoked obesity, we dissected visceral and nonvisceral fat depots from all experimental groups and weighted them in correlation to the body weight of each individual mouse. MT mice had a significant increased weight of all white adipose tissues, in both sexes, compared to CoD-fed WT mice and when they were fed a WeD the resulting adiposity accumulation was even greater. Obesity and metabolic disorders are associated with adipocyte size and turnover [10] and indeed we found adipocyte hypertrophy in ScAT and PgAT in CoD-fed MT and WeD-fed mice in both sexes. The increased accumulation of lipids suggested that MT mice could have impairments in lipid metabolism, hence dyslipidaemia. Hyperlipidaemia is the most common form of dyslipidaemia, characterised by elevated levels of triglycerides, cholesterol and lipoproteins in the blood [117]. In 12-week-old mice, all groups demonstrated a significant increase in basal triglycerides and cholesterol compared to CoD-fed WTs, except for WeD-fed female WTs. During CoD the hypertriglyceridemia appeared earlier in females than males. An opposite trend was found for the development of hypercholesterolemia. Noteworthy, the pattern of dyslipidaemia found in WeD-fed WT mice was very similar to the CoD-fed MT until the end of the study. Finally, the synergistic effect of combining genotype and diet resulted in the worst hyperlipidaemia levels. Similar results have been also described in patients with certain polymorphisms in the *Snap25* gene, treated with antipsychotic drugs for schizophrenia, where elevated serum triglycerides levels and body weight gain have been described [118,119]. We have also analysed humoral factors such as leptin and ghrelin since it is known that their abnormal release is associated with obesity and metabolic dysfunctions [115]. Measurements of basal serum leptin levels revealed that in CoD-fed MT females they were significantly higher than WTs. Again, the effect of both SNAP-25b-deficiency and diet resulted in the worst phenotype. Ghrelin was decreased in all experimental groups compared to CoD-fed WTs, in accordance with conditions associated to metabolic impairment [120,121].

4.1.4 SNAP-25b-deficiency induces liver dysfunction

The increased levels of serum leptin led us to study leptin resistance in the liver, as it is a target tissue during metabolic disease [115]. Independently of sex, the long isoform of the ObR, ObRb, was down-regulated compared to CoD-fed WTs in all experimental groups. Interestingly, the short isoform of the receptor, ObRa, was detectable only in MT mice, maybe as an attempt to compensate for decreased ObRb expression. We have also determined lipid accumulation in liver and found that SNAP-25b-deficiency was sufficient to turn the liver into a hepatic steatosis status, similarly to WeD-fed WT animals. When the mutation was combined with WeD the liver disease turned to severe fatty liver disease. The hypothalamus has a major role into hepatic lipid metabolism and storage via the autonomic nervous system and it is believed that increased sympathetic activity induces lipid accumulation in the liver [122,123]. In our SNAP-25b-deficient mice it is plausible that the impaired neuroexocytosis from autonomic nerves causes liver steatosis.

To summarise, in Paper I we have tested if a small genetic modification in the SNARE complex (*i. e.*, replacing SNAP-25b with SNAP-25a), likely resulting in altered release of hormones, like insulin, could provoke metabolic syndrome in mice. Indeed, already at 12 weeks of age, mice carrying this mutation developed symptoms of metabolic disease, which became full-blown when fed the WeD. It is tempting to hypothesise that also in humans such mutations, combined with an unhealthy diet and a sedentary life could be part of the triggering factors for the development of metabolic disease.

4.2 PAPER II

In Paper I, we have studied the metabolic consequences of the lack of SNAP-25b *in vivo* and found it correlated to an increased insulin secretion during GTT. In Paper II, we funnelled down to investigate the effect of SNAP-25b-deficiency on insulin secretion from beta cells and islet physiology, hypothesizing that this could contribute to development of the metabolic syndrome [8]. We expected SNAP-25b-deficiency in beta cells to lead to a facilitated release, primarily affecting the dynamics of different pools of insulin granules [42,53]. Indeed, we found an increased insulin secretion phenotype, however, this was instead associated with poorly controlled Ca^{2+} dynamics among beta cells in SNAP-25b-deficient mice. These results indicated additional functions of the SNAP-25 isoforms beyond their classical role in the SNARE complex mediating membrane fusion. Coordination of Ca^{2+} oscillations in beta cells is fundamental for a physiological release of insulin and disruptions of this mechanism can lead to development of insulin resistance and obesity [124]. The experiments were run in 12-week-old male and female, WT and MT mice on CoD.

4.2.1 SNAP-25b-deficiency increases insulin secretion and affects islet morphology

Although SNAP-25b is the least abundant isoform in the endocrine beta cell [46,53], we found increased insulin secretion in islets isolated from MT mice compared to WTs when perifused with 11 mM glucose and 25 mM KCl. This secretion pattern was also found *in vivo* when the mice were challenged with a 15 min-long GTT. Serum insulin levels in MT mice were higher at all time points, although the blood glucose remained unchanged compared to the WTs. Interestingly, the WT females were found to have consistently lower serum insulin levels compared to WT males and therefore MT females demonstrated hyperinsulinemia and hyperglycaemia compared to their corresponding WT littermates. These results were also supported by the calculation of $HOMA_{IR}$, an estimation of insulin resistance which indicated that WT females were more sensitive to insulin compared to WT males, probably due to different body composition.

To investigate if the increased insulin secretion was attributed to altered islet morphology and cell distribution, we analysed pancreatic sections immunolabelled for insulin and glucagon as well as H&E labelled sections. First of all, we noticed the same characteristic spatial distribution of alpha and beta cells in SNAP-25b-deficient islets as in the WTs. More detailed analyses revealed that MT males had an increased number of insulin-positive cells per islet as well as larger islets compared to WT males, which could in part explain the increased insulin secretion. The number of alpha cells in islets was identical in WT and MT islets. Remarkably, islets from WT females contained more beta cells compared to WT males, although the individual beta cells were smaller in size, as determined by membrane capacitance measurements. WT females were found to have the highest number of islets among the groups. No signs of apoptosis were detected in beta cells in MT mice as compared to WTs. Taken together, the differences found between WT males and females is maybe attributed to the compensation of energy demands females encounter in case of pregnancy [125].

4.2.2 SNAP-25b-deficiency does not influence Ca^{2+}-sensitivity or rate of exocytosis

As we hypothesised that the increased insulin secretion in MT islets was dependent on less stable SNARE complexes that could facilitate exocytosis, we performed experiments with slow photo-release of caged Ca^{2+} in beta cells with patch clamp. To do so we took advantage of the pancreatic tissue slice technique, where it is possible to get access to populations of beta cells resident in the islet core and beta cells are surrounded by their natural environment, the exocrine pancreas [90]. Slow photo-release of caged Ca^{2+} produces a ramp-like increase in

$[Ca^{2+}]_i$ up to a threshold value (Ca_{tr}) that triggers exocytosis, measured as a biphasic increase in membrane capacitance [126]. To our surprise, when $[Ca^{2+}]_i$ raised no difference was found either in Ca^{2+} sensitivity, amplitude or rate of exocytosis between WT and MT beta cells. Therefore, the increased secretion found *in vivo* and *in vitro* could not only be dependent on the stability of SNARE complexes formed with either isoforms.

4.2.3 SNAP-25b is necessary for accurate regulation of Ca^{2+} dynamics in beta cells

We hypothesised that the different SNAP-25 isoforms might act differently on upstream targets involved in insulin exocytosis. It is known that SNAP-25, also in combination with syntaxin, binds to a number of proteins important for ion trafficking and electrical activity in excitable cells, such as VDCCs and K^+ channels [54–56,127–129].

We therefore explored if SNAP-25b-deficiency affected intracellular Ca^{2+} dynamics in beta cells using functional Ca^{2+} imaging on pancreatic tissue slices. When we stimulated the islets with 12 mM glucose, the initiation phase started with its characteristic progressive heterogeneous recruitment of beta cells [90] and beta cell activation time spanned from 1 to 6 min in all experimental groups. Interestingly, in islets from MT mice a subgroup of beta cells responded earlier, which reflected an overall less regulated and faster glucose-induced Ca^{2+} response. When we removed high glucose, the beta cells deactivation started after 2-3 min and propagated within the islet with a high grade of heterogeneity from islet to islet, sometimes lasting even longer than 20 min. A detailed analysis revealed that in males, beta cells in MT islets experienced a deactivation process significantly longer than WTs.

A consistent part of the Ca^{2+} imaging analysis was dedicated to the “active” stimulatory phase in beta cells which was reached after 7-15 min of 12 mM glucose exposure and is predominantly characterised by sustained oscillatory Ca^{2+} activity, superimposed on an elevated basal Ca^{2+} level [90]. First of all, we calculated the mean frequency and duration of individual Ca^{2+} oscillations for all experimental groups and found no significant differences except for increased mean pulse duration in MT females compared to WTs. However, when we calculated the mean coactivity we disclosed a low grade of synchronicity between beta cells within MT islets compared to WTs in both males and females, indicating a weaker collective control of Ca^{2+} elevations. These characteristics in MT islets together with the morphological changes observed at least in males suggested lesions in the quality of beta cell-to-cell interaction and hence possibly influencing hormonal secretion. We studied the functional connectivity profiles in all subgroups using analytical tools from the theory of the complex network [130]. Previous studies on beta cell networks indicated that they form

heterogeneous, efficient and clustered architecture [131–134]. When we calculated the modularity, we found that functional networks extracted from MT males were more segregated compared to WTs. The modular connectivity could be dependent on beta cell hyperplasia found in MT males coupled with looser connections between beta cells as the gap junction conductance, measured by patch clamp, tended to be decreased in MT compared to WT cells. Also, the spatial distribution of frequencies within the islet indicated a segregation of beta cell activity in MTs. During the last years, correct inter-beta-cell-connectivity within the islet has been described as fundamental for the generation of coordinated rhythmic insulin release and this complex network can be disrupted during the pathogenesis of T2D [99,101–103,135]. In our MT mice, we found increased glucose-induced insulin release associated with less synchronised Ca^{2+} oscillations, which is in line with previous results from other groups [81,99,100]. Although we have not focused our research on pulsatile insulin secretion, a trait impaired during the progression of T2D, this might be a possible effect behind the deregulated Ca^{2+} dynamics, leading to progressive insulin resistance.

Altogether, the results in Paper II indicate that, although SNAP-25b is the minor isoform in beta cells, its function cannot be replaced by SNAP-25a. Islets lacking SNAP-25b were found to secrete high levels of insulin upon glucose stimulation and this was associated with derangement in islet morphology and less well controlled Ca^{2+} oscillations in beta cells. The lost regulation of beta cell activity behind the increased insulin secretion can, in a long term, provoke insulin resistance in peripheral tissues, hence contributing to the development of metabolic syndrome characterised in Paper I.

4.3 PAPER III

In Paper II we have shown that SNAP-25b-deficiency in islets results in a phenotype not entirely dependent on mechanisms downstream Ca^{2+} entry, suggesting other roles of the SNAP-25 isoforms "outside" the core SNARE complex. It has previously been demonstrated that SNAP-25b confers an increased thermostability to the complex compared to SNAP-25a [51,52], possibly forming more hydrogen bonds between the proteins. However, during physiological conditions, differences in thermostability above 70 °C are not relevant, but the additional chemical bonds can change the tertiary structure of the four-alpha-helical bundle of the SNARE complex. Therefore, it is plausible that SNAP-25a and SNAP-25b might differently mediate interactions with binding partners. To investigate this hypothesis, we run immunoprecipitations of SNAP-25-containing complexes in the hippocampus from WT and MT mice. The hippocampus is one of the few brain areas where SNAP-25a is almost completely replaced by the SNAP-25b isoform in adulthood [43], thus we selected to work with

this region. We focused on interactions with the SNARE partners, syntaxin 1 and VAMP-2, as well as with proteins important for initiating or inhibiting membrane fusion events, such as Munc18-1 and the Gβγ subunits of the heterotrimeric G proteins, respectively [31,68,70,136].

First of all, we quantified the total protein expression levels in hippocampi from WT and MT mice and found no significant difference in SNAP-25, syntaxin 1, VAMP-2, Munc18-1 and Gβ1-4 proteins. We then continued by immunoprecipitating molecular complexes using SNAP-25 as bait. We could not detect any changes in the amount of the SNARE complex proteins, syntaxin 1 and VAMP-2, bound to either SNAP-25 isoform whereas an effect was detected for Munc18-1 and Gβγ. SNAP-25a was able to attract only half of the amount of Munc18-1 compared to SNAP-25b, maybe reflecting a decreased capability of SNAP-25a-containing SNARE complexes to be in a "primed" state. Interestingly, two bands appeared to be immunoreactive to the Gβ1-4 antibody in both WT and MT hippocampi (several control experiments for testing the specificity of the antibody were carried out). The heavier band was more diffuse, suggesting the presence of possible post-transcriptional modifications of this protein, the lighter band appeared instead sharper and more defined, thus likely indicating a unique population of unmodified protein. It is known that in mouse hippocampus the majority of Gβ isoforms consists of the Gβ1, Gβ2 and Gβ4 [137]. To investigate which isoforms interacted with SNAP-25, we analysed the two bands by mass spectrometry and found Gβ2 and Gβ1 in the heavier and lighter band, respectively. No detectable levels of Gβ4 were found to interact with SNAP-25 in hippocampus. Not much is known about the functions of the different Gβ isoforms in synaptic inhibition except that in rat superior cervical ganglion neurons Gβ1 and Gβ2 account for the majority of voltage-dependent inhibition of N-type Ca^{2+} channels [138]. SNAP-25 interaction to the Gβγ is a relatively new and very interesting area of research since it appears to be implicated in transient transmitter-mediated presynaptic inhibition and induction of presynaptic long-term depression, important for memory and learning processes [72]. The mechanism of action has been proposed to involve the vesicle-associated protein synaptotagmin, which can approach the SNARE complex and initiate exocytosis upon appropriate Ca^{2+} concentrations, but when a GPCR is activated, the Gβγ subunit competes with synaptotagmin for binding to the SNARE complex, thus inhibiting fusion [71] (Figure 3). With our experimental approach, we found that SNAP-25a was able to attract a significantly lower amount of Gβ2 compared to SNAP-25b, maybe meaning its decreased efficiency in inhibiting exocytosis upon certain stimuli. Moreover, proximity ligation assays on hippocampal sections confirmed that the interaction of the SNAP-25 isoforms and the Gβγ was of a direct nature.

To summarise, it is plausible that the SNAP-25 isoforms might provide different regulation of membrane fusion events, by modified interaction with other SNARE-binding proteins. This could in part explain learning and memory dysfunctions associated to the SNAP-25b-deficient mice [52] as well as increased hormonal secretion from peripheral tissues (Paper I and II). Yet, more functional experiments are needed in order to further investigate these mechanisms.

5 CONCLUSIONS

Stimulus-dependent regulated membrane fusion is a complex physiological process that enables secretory cells, such as neurons and beta cells, to secrete neurotransmitters/hormones upon appropriate stimuli. SNAP-25, together with syntaxin 1 and VAMP-2, forms the core SNARE complex, implicated in the last steps of exocytosis fusing the vesicle/granule and cell plasma membranes. SNAP-25 exists as two developmentally regulated splicing variants, SNAP-25a and SNAP-25b, differing in only 9 out of 206 amino acids. Both SNAP-25 proteins can form SNARE complexes but their different roles in membrane fusion are not much investigated.

By using a SNAP-25b-deficient mouse model, this thesis has focused on studying the functions of the SNAP-25 isoforms in glucose and insulin homeostasis *in vivo*. Normally both isoforms participate in the SNARE complex and thus exocytosis, but when mice expressed only SNAP-25a, this resulted in development of metabolic syndrome in adulthood which was more exacerbated when combined with a high fat/high sucrose diet. Symptoms characteristic of metabolic disease included hyperinsulinemia, insulin resistance, hyperglycaemia, liver steatosis and adipocyte hypertrophy. SNAP-25b-deficiency resulted in increased insulin secretion, not merely dependent on mechanisms downstream the Ca^{2+} entry but instead associated to desynchronization of Ca^{2+} dynamics among beta cells. The disrupted beta cell networks, together with changes in the islet morphology in MTs contributed to the secretion phenotype. Moreover, we found different binding abilities of the SNAP-25 isoforms for proteins modulating membrane fusion, a result that needs to be further investigated.

In conclusion, the correct function of the exocytosis machinery is important for health and insults to genes coding for its protein components can provoke metabolic syndrome. The SNAP-25 splicing variants play different roles in secretion, and as we experimentally proved they cannot be interchangeable, without impairing insulin secretion. In the future it would be of interest to characterise SNAP-25 isoforms levels in islets from other models of metabolic disease, as well as from T2D donors for clinical implications. Moreover, we propose the SNAP-25b-deficient mouse as a useful model for studies on development and progression of the metabolic syndrome and for testing therapeutic interventions.

6 ACKNOWLEDGEMENTS

This thesis work was performed at the Rolf Luft Center for Diabetes and Endocrinology at the Department of Molecular Medicine and Surgery at Karolinska Institutet in Solna. During these years, I have met many talented and helpful people who made my PhD journey one of the best experiences of my life. In particular, I would like to express my deepest gratitude to:

Christina Bark, my main supervisor. You have introduced me to a very exciting field of research, I have learnt a lot from you, in terms of science and life in general. Thank you for always finding the solution to the problem in the most practical way! You have constantly supported me by being there when I needed, I will never forget it. THANK YOU!

Marjan Slak Rupnik, my co-supervisor. You are a driven and positive person, who engaged me into islet physiology. Thank you for letting me work in your research unit in Slovenia and for sharing your wide knowledge.

Kerstin Brismar, my co-supervisor. You have a true passion for science and research and you are a kind-hearted and helpful person. Thanks for always giving a "clinical" perspective to my results.

Gilberto Fisone, thanks for the fruitful conversations we had during my PhD journey and thanks for your advices.

Essam Refai, the Egyptian disaster, thanks for guiding me during these years and for being a real friend, thanks for the numerous times you helped me! Without you this journey would have been much more difficult.

Ismael Valladolid-Acebes, my colleague and friend, thanks for sharing your passion and enthusiasm for science, you have been my teacher in the lab, always helpful and kind! Also, thanks for being a good party mate and for providing good tortillas and coccinillo. **Pauline Vercruisse**, it was fun and useful working with you and I now know how to dissect the soleus from the mouse leg thanks to you! I like your French accent and your perseverance. **Irfan Jadoon**, thanks for sharing your genuine interest in science and helping me with the experiments.

Special thanks go to all my fantastic "big-lab" mates: **Sampath Narayanan** and **Anette Landström**, it was nice having you as my office-mates, I hope I didn't bother you too much (I know I actually did). **Jacob Grünler**, thanks for being such a nice person and for all the times you helped me using lab equipment. Sorry for annoying you for the liquid nitrogen so often. **Michael Tekle**, "Michele", always smiling, making jokes and taking care of my plants during Christmas/summer, thanks! **Ileana Botusan**, **Ishrath Ansurudeen**, **Elisabeth Noren-Krog**, **Magnus Bentinger**, **Xiao-Wei Zheng**, thanks for your help and nice discussions about science and life! **Sofie Eliasson** and **Cheng Xu**, it has been my pleasure having you as PhD-mates.

Thank you, **Sergiu Catrina** for sharing your knowledge in science and for your good sense of humour. Thank you **Gustav Dallner** for being an inspiring person and teaching me the healthy properties of antioxidants in wine, the glass is always full if you are around.

My sincere gratitude goes to my colleagues in Maribor, Slovenia: **Maša Skelin Klemen**, **Marko Gosak**, **Lidija Križančić Bombek**, **Jurij Dolenšek**, **Andraž Stožer**, **Rudi Mlakar**, **Viljem Pohorec**. Thanks for teaching me the cool techniques developed in your lab and for sharing your vast knowledge in beta cell physiology. I appreciated your efforts in making me feel at ease during my trips to Maribor.

Thanks to the Rolf Luft Italian mates: **Marianna Del Sole**, **Noah Moruzzi**, **Elisabetta Darè**, **Massimiliano Ria** for supporting me and making me feel at home.

Subu Surendran Rajasekaran, **Pim van Krieken**, **Meike Paschen**, **Yue Shi**, **Robin Fröbon**, **Karin Åvall**, **Saad Al-Qahtani**, the PhD students at the Rolf Luft Center, thanks for the fruitful discussions during the Journal Clubs and the nice dinners, I very much enjoyed your company.

Concepcion Fernandez Garcia-Prieto, "Conchita", thanks for being my sincere friend, I love your enthusiasm and good mood. Thanks for cheering me up when I needed. **Yan Xiong**, **Anya Voznesenskaya**, **Teresa Pereira**, **Tomas Alanentalo**, **Stefan Jacob**, **Galyna Bryzgalova**, **Tilo Moede**, **Andrea Dicker**, **Montse Visa Majoral**, **Christopher Barker**, **Neil Portwood**, **Lars Selander**, **Martin Köhler** and **Yvonne Strömberg**, thank you all for helping me during these years and for the nice discussions and parties!

Thais Soprani Ayala, **Fernando Tessaro**, **Anderson Daniel Ramos**, **Eduardo Nolasco**, **Karin Tiago Dos Santos**, the former Brazilian crew in the lab, thanks for always cheering me up with your enthusiasm and joyful attitude, it was nice meeting you all and I wish I will meet you again!

Katarina Breitholtz, **Ann-Britt Wikström**, **Britt-Marie Witasp** and colleagues, thanks for helping me with forms/documents/certifications, you made my days easier. Thanks to the IT personnel, especially **Jan-Erik Kaare** for saving the life of my computer several times!

Tomas Hökfelt, **Csaba Adori** and **Ida Nilsson**, thanks for your collaborative efforts and for sharing your vast knowledge in the field of neuroscience.

Thanks **Per-Olof Berggren** for your collaboration and comments on the manuscript. **Lisa Juntti-Berggren**, thanks for all the hilarious discussions we had about "the tough process of publishing manuscripts nowadays".

AKM animal house staff, thanks for taking good care of my mice during these years with an amazing professionality.

To my "Stockholm" friends: **Aileen**, **Aida**, **Christine**, **João**, **Daniela**, **Domenico**, **Silvia**, **Roberta**, **Ben**, **Marta**, **Apo**, **Roshan**, **Martin**, **Lucia**, **Gianna**, **Anil**, **Helene**, **Daniel**,

Franzi, **Dave**, **Marika**, **Mathias**, **Karolina**, **Erik** and **Esther**, thanks for the good time spent together in Sweden and for all the MF pubs.

To my friends in Italy who have been mostly involved in my "PhD drama" (**Daniele**, **Giovanna**, **Roberta**, **Simona**, **Anna**, **Luca**, **Nick**, **Vale**, **Silvia**, **Sara**), thanks for your friendship and for supporting me in the difficult moments and being there when I needed to have fun, I love you all!

Infine vorrei ringraziare la mia straordinaria famiglia: **Mamma**, **Papà**, **Grazia**, **Nonna** e **Mino** per amarmi e incoraggiarmi in ogni momento della mia vita, soprattutto in quelli difficili. Senza il vostro supporto non sarei la persona che sono oggi. Grazie per credere in me! **Mino,** grazie per essere stato (e lo sarai ancora per molto tempo!) il mio mentore/consigliere/amico/compagno di vita durante questi anni.

This research was supported by grants from the Family Erling-Persson Foundation, Karolinska Institutet funds, the Magnus Bergvalls Foundation, the Gun and Bertil Stohnes Foundation, Längmanska Kulturfonden, the Novo Nordisk Foundation, the Fogelströms Foundation, and the Sven Mattssons Foundation, Sigurd and Elsa Goljes Foundation and the Slovenian Research Agency (Program P3–0396). Research visits to Slovenia were supported by a Rolf Luft Fellowship, Fernströms Foundation and KI travel funds for PhD students.

7 REFERENCES

1. Alberti, K. G. M. M., Zimmet, P. & Shaw, J. Metabolic syndrome-a new world-wide definition. A Consensus Statement from the International Diabetes Federation. *Diabet. Med.* **23,** 469–480 (2006).

2. Aschner, P. Metabolic syndrome as a risk factor for diabetes. *Expert Rev. Cardiovasc. Ther.* **8,** 407–412 (2010).

3. Gao, Q. & Horvath, T. L. Neurobiology of Feeding and Energy Expenditure. *Annu. Rev. Neurosci.* **30,** 367–398 (2007).

4. Bartness, T. J., Keen-Rhinehart, E., Dailey, M. J. & Teubner, B. J. Neural and hormonal control of food hoarding. *AJP Regul. Integr. Comp. Physiol.* **301,** R641–R655 (2011).

5. Lin, H. V. & Accili, D. Hormonal Regulation of Hepatic Glucose Production in Health and Disease. *Cell Metab.* **14,** 9–19 (2011).

6. Cerf, M. E. Beta Cell Dysfunction and Insulin Resistance. *Front. Endocrinol.* **4,** 37 (2013).

7. Cerasi, E. & Luft, R. THE PLASMA INSULIN RESPONSE TO GLUCOSE INFUSION IN HEALTHY SUBJECTS AND IN DIABETES MELLITUS. *Eur. J. Endocrinol.* **55,** 278–304 (1967).

8. Seino, S., Shibasaki, T. & Minami, K. Dynamics of insulin secretion and the clinical implications for obesity and diabetes. *J. Clin. Invest.* **121,** 2118–2125 (2011).

9. Sun, K., Kusminski, C. M. & Scherer, P. E. Adipose tissue remodeling and obesity. *J. Clin. Invest.* **121,** 2094–2101 (2011).

10. Arner, P. *et al.* Dynamics of human adipose lipid turnover in health and metabolic disease. *Nature* **478,** 110–113 (2011).

11. Cline, G. W. *et al.* Impaired Glucose Transport as a Cause of Decreased Insulin-Stimulated Muscle Glycogen Synthesis in Type 2 Diabetes. *N. Engl. J. Med.* **341,** 240–246 (1999).

12. Muoio, D. M. & Newgard, C. B. Mechanisms of disease: Molecular and metabolic mechanisms of insulin resistance and β-cell failure in type 2 diabetes. *Nat. Rev. Mol. Cell Biol.* **9,** 193–205 (2008).

13. Mazen, I., El-Gammal, M., Abdel-Hamid, M. & Amr, K. A novel homozygous missense mutation of the leptin gene (N103K) in an obese Egyptian patient. *Mol. Genet. Metab.* **97,** 305–308 (2009).

14. Südhof, T. C. & Rothman, J. E. Membrane fusion: grappling with SNARE and SM proteins. *Science* **323,** 474–477 (2009).

15. Halban, P. A. & Irminger, J. C. Sorting and processing of secretory proteins. *Biochem. J.* **299 (Pt 1),** 1–18 (1994).

16. De Camilli, P. & Jahn, R. Pathways to Regulated Exocytosis in Neurons. *Annu. Rev. Physiol.* **52,** 625–645 (1990).

17. Thomas-Reetz, A. *et al.* A gamma-aminobutyric acid transporter driven by a proton

pump is present in synaptic-like microvesicles of pancreatic beta cells. *Proc. Natl. Acad. Sci.* **90,** 5317–5321 (1993).

18. Barg, S. Mechanisms of Exocytosis in Insulin-Secreting B-Cells and Glucagon-Secreting A-Cells. *Pharmacol. Toxicol.* **92,** 3–13 (2003).

19. Martin, T. F. J. Tuning exocytosis for speed: fast and slow modes. *Biochim. Biophys. Acta - Mol. Cell Res.* **1641,** 157–165 (2003).

20. Schneggenburger, R. & Rosenmund, C. Molecular mechanisms governing Ca^{2+} regulation of evoked and spontaneous release. *Nat. Neurosci.* **18,** 935–941 (2015).

21. Bratanova-Tochkova, T. K. *et al.* Triggering and Augmentation Mechanisms, Granule Pools, and Biphasic Insulin Secretion. *Diabetes* **51,** S83–S90 (2002).

22. Becherer, U. & Rettig, J. Vesicle pools, docking, priming, and release. *Cell Tissue Res.* **326,** 393–407 (2006).

23. Söllner, T., Bennett, M. K., Whiteheart, S. W., Scheller, R. H. & Rothman, J. E. A protein assembly-disassembly pathway in vitro that may correspond to sequential steps of synaptic vesicle docking, activation, and fusion. *Cell* **75,** 409–418 (1993).

24. Söllner, T. *et al.* SNAP receptors implicated in vesicle targeting and fusion. *Nature* **362,** 318–324 (1993).

25. Rutter, G. A. & Tsuboi, T. Kiss and run exocytosis of dense core secretory vesicles. *Neuroreport* **15,** 79–81 (2004).

26. Jarvis, S. E. & Zamponi, G. W. Masters or slaves? Vesicle release machinery and the regulation of presynaptic calcium channels. *Cell Calcium* **37,** 483–488 (2005).

27. Südhof, T. C. Synaptotagmins: Why So Many? *J. Biol. Chem.* **277,** 7629–7632 (2002).

28. Turner, K. M., Burgoyne, R. D. & Morgan, A. Protein phosphorylation and the regulation of synaptic membrane traffic. *Trends Neurosci.* **22,** 459–464 (1999).

29. Südhof, T. C. The Molecular Machinery of Neurotransmitter Release (Nobel Lecture). *Angew. Chemie Int. Ed.* **53,** 12696–12717 (2014).

30. Kaiser, C. A. & Schekman, R. Distinct sets of SEC genes govern transport vesicle formation and fusion early in the secretory pathway. *Cell* **61,** 723–733 (1990).

31. Hata, Y., Slaughter, C. A. & Südhof, T. C. Synaptic vesicle fusion complex contains unc-18 homologue bound to syntaxin. *Nature* **366,** 347–351 (1993).

32. Bennett, M., Calakos, N. & Scheller, R. Syntaxin: a synaptic protein implicated in docking of synaptic vesicles at presynaptic active zones. *Science* **257,** 255–259 (1992).

33. Oyler, G. A. *et al.* The identification of a novel synaptosomal-associated protein, SNAP-25, differentially expressed by neuronal subpopulations. *J. Cell Biol.* **109,** 3039–3052 (1989).

34. Trimble, W. S., Cowan, D. M. & Scheller, R. H. VAMP-1: a synaptic vesicle-associated integral membrane protein. *Proc. Natl. Acad. Sci.* **85,** 4538–4542 (1988).

35. Gonzalo, S., Greentree, W. K. & Linder, M. E. SNAP-25 Is Targeted to the Plasma Membrane through a Novel Membrane-binding Domain. *J. Biol. Chem.* **274,** 21313–

21318 (1999).

36. Lane, S. R. & Liu, Y. Characterization of the palmitoylation domain of SNAP-25. *J. Neurochem.* **69,** 1864–1869 (1997).

37. Sutton, R. B., Fasshauer, D., Jahn, R. & Brunger, A. T. Crystal structure of a SNARE complex involved in synaptic exocytosis at 2.4 A resolution. *Nature* **395,** 347–353 (1998).

38. Chen, Y. A. & Scheller, R. H. SNARE-mediated membrane fusion. *Nat. Rev. Mol. Cell Biol.* **2,** 98–106 (2001).

39. Washbourne, P. *et al.* Genetic ablation of the t-SNARE SNAP-25 distinguishes mechanisms of neuroexocytosis. *Nat. Neurosci.* **5,** 19–26 (2002).

40. Bark, I. C. Structure of the Chicken Gene for SNAP-25 Reveals Duplicated Exons Encoding Distinct Isoforms of the Protein. *J. Mol. Biol.* **233,** 67–76 (1993).

41. Bark, I. C. & Wilson, M. C. Human cDNA clones encoding two different isoforms of the nerve terminal protein SNAP-25. *Gene* **139,** 291–292 (1994).

42. Sørensen, J. B. *et al.* Differential Control of the Releasable Vesicle Pools by SNAP-25 Splice Variants and SNAP-23. *Cell* **114,** 75–86 (2003).

43. Bark, I. C., Hahn, K. M., Ryabinin, A. E. & Wilson, M. C. Differential expression of SNAP-25 protein isoforms during divergent vesicle fusion events of neural development. *Proc. Natl. Acad. Sci.* **92,** 1510–1514 (1995).

44. Boschert, U. *et al.* Developmental and plasticity-related differential expression of two SNAP-25 isoforms in the rat brain. *J. Comp. Neurol.* **367,** 177–193 (1996).

45. Grant, N. J. *et al.* Differential Expression of SNAP-25 Isoforms and SNAP-23 in the Adrenal Gland. *J. Neurochem.* **72,** 363–372 (2002).

46. Gonelle-Gispert, C. *et al.* SNAP-25a and -25b isoforms are both expressed in insulin-secreting cells and can function in insulin secretion. *Biochem. J.* **339 (Pt 1),** 159–165 (1999).

47. Yamamori, S. *et al.* Differential expression of SNAP-25 family proteins in the mouse brain. *J. Comp. Neurol.* **519,** 916–932 (2011).

48. Bark, C. *et al.* Developmentally Regulated Switch in Alternatively Spliced SNAP-25 Isoforms Alters Facilitation of Synaptic Transmission. *J. Neurosci.* **24,** 8796–8805 (2004).

49. Sharma, M. *et al.* CSPα knockout causes neurodegeneration by impairing SNAP-25 function. *EMBO J.* **31,** 829–841 (2012).

50. Sharma, M., Burré, J. & Südhof, T. C. CSPα promotes SNARE-complex assembly by chaperoning SNAP-25 during synaptic activity. *Nat. Cell Biol.* **13,** 30–39 (2011).

51. Nagy, G. *et al.* Alternative splicing of SNAP-25 regulates secretion through nonconservative substitutions in the SNARE domain. *Mol Biol Cell* **16,** 5675–5685 (2005).

52. Johansson, J. U. *et al.* An Ancient Duplication of Exon 5 in the Snap25 Gene Is Required for Complex Neuronal Development/Function. *PLoS Genet.* **4,** e1000278

(2008).

53. Jeans, A. F. *et al.* A dominant mutation in Snap25 causes impaired vesicle trafficking, sensorimotor gating, and ataxia in the blind-drunk mouse. *Proc. Natl. Acad. Sci.* **104,** 2431–2436 (2007).

54. Ji, J. *et al.* Modulation of L-Type Ca^{2+} Channels by Distinct Domains Within SNAP-25. *Diabetes* **51,** 1425–1436 (2002).

55. Rettig, J. *et al.* Isoform-specific interaction of the alpha1A subunits of brain Ca^{2+} channels with the presynaptic proteins syntaxin and SNAP-25. *Proc. Natl. Acad. Sci.* **93,** 7363–7368 (1996).

56. Toft-Bertelsen, T. L., Ziomkiewicz, I., Houy, S., Pinheiro, P. S. & Sorensen, J. B. Regulation of Ca^{2+} channels by SNAP-25 via recruitment of syntaxin-1 from plasma membrane clusters. *Mol. Biol. Cell* **27,** 3329–3341 (2016).

57. Novick, P. & Schekman, R. Secretion and cell-surface growth are blocked in a temperature-sensitive mutant of Saccharomyces cerevisiae. *Proc. Natl. Acad. Sci.* **76,** 1858–1862 (1979).

58. Verhage, M. *et al.* Synaptic assembly of the brain in the absence of neurotransmitter secretion. *Science* **287,** 864–869 (2000).

59. Dulubova, I. *et al.* A conformational switch in syntaxin during exocytosis: role of munc18. *EMBO J.* **18,** 4372–4382 (1999).

60. Misura, K. M., Scheller, R. H. & Weis, W. I. Three-dimensional structure of the neuronal-Sec1-syntaxin 1a complex. *Nature* **404,** 355–362 (2000).

61. Yamaguchi, T. *et al.* Sly1 Binds to Golgi and ER Syntaxins via a Conserved N-Terminal Peptide Motif. *Dev. Cell* **2,** 295–305 (2002).

62. Dulubova, I. *et al.* How Tlg2p/syntaxin 16 'snares' Vps45. *EMBO J.* **21,** 3620–2631 (2002).

63. Betke, K. M., Wells, C. A. & Hamm, H. E. GPCR mediated regulation of synaptic transmission. *Prog. Neurobiol.* **96,** 304–321 (2012).

64. Simon, M., Strathmann, M. & Gautam, N. Diversity of G proteins in signal transduction. *Science* **252,** 802–808 (1991).

65. Kajikawa, Y., Saitoh, N. & Takahashi, T. GTP-binding protein subunits mediate presynaptic calcium current inhibition by GABAB receptor. *Proc. Natl. Acad. Sci.* **98,** 8054–8058 (2001).

66. Takahashi, T., Forsythe, I. D., Tsujimoto, T., Barnes-Davies, M. & Onodera, K. Presynaptic Calcium Current Modulation by a Metabotropic Glutamate Receptor. *Science* **274,** 594–597 (1996).

67. Fernández-Alacid, L. *et al.* Subcellular compartment-specific molecular diversity of pre- and post-synaptic GABA B -activated GIRK channels in Purkinje cells. *J. Neurochem.* **110,** 1363–1376 (2009).

68. Blackmer, T. *et al.* G protein betagamma subunit-mediated presynaptic inhibition: regulation of exocytotic fusion downstream of Ca^{2+} entry. *Science* **292,** 293–297 (2001).

69. Blackmer, T. *et al.* G protein βγ directly regulates SNARE protein fusion machinery for secretory granule exocytosis. *Nat. Neurosci.* **8,** 421–425 (2005).

70. Gerachshenko, T. *et al.* Gβγ acts at the C terminus of SNAP-25 to mediate presynaptic inhibition. *Nat. Neurosci.* **8,** 597–605 (2005).

71. Yoon, E.-J., Gerachshenko, T., Spiegelberg, B. D., Alford, S. & Hamm, H. E. Gbeta Interferes with Ca^{2+}-Dependent Binding of Synaptotagmin to the Soluble N-Ethylmaleimide-Sensitive Factor Attachment Protein Receptor (SNARE) Complex. *Mol. Pharmacol.* **72,** 1210–1219 (2007).

72. Zhang, X., Upreti, C. & Stanton, P. K. Gβγ and the C Terminus of SNAP-25 Are Necessary for Long-Term Depression of Transmitter Release. *PLoS One* **6,** e20500 (2011).

73. Atwood, B. K., Lovinger, D. M. & Mathur, B. N. Presynaptic long-term depression mediated by Gi/o-coupled receptors. *Trends Neurosci.* **37,** 663–673 (2014).

74. Zhao, Y., Fang, Q., Straub, S. G., Lindau, M. & Sharp, G. W. G. Noradrenaline inhibits exocytosis via the G protein βγ subunit and refilling of the readily releasable granule pool via the α i1/2 subunit. *J. Physiol.* **588,** 3485–3498 (2010).

75. Langerhans, P. Beiträge zur mikroskopischen anatomie der bauchspeicheldrüse. Inaugural dissertation. *Berlin: Gustav Lange* (1869).

76. Rupnik, M. The physiology of rodent beta-cells in pancreas slices. *Acta Physiol.* **195,** 123–138 (2009).

77. Miller, K. *et al.* Islet Formation during the Neonatal Development in Mice. *PLoS One* **4,** e7739 (2009).

78. Dolenšek, J., Rupnik, M. S. & Stožer, A. Structural similarities and differences between the human and the mouse pancreas. *Islets* **7,** e1024405 (2015).

79. Orci, L. & Unger, R. FUNCTIONAL SUBDIVISION OF ISLETS OF LANGERHANS AND POSSIBLE ROLE OF D CELLS. *Lancet* **306,** 1243–1244 (1975).

80. Grube, D. & Bohn, R. The microanatomy of human islets of Langerhans, with special reference to somatostatin D-cells. *Arch. histol. Jap.* **46,** 327–253 (1983).

81. Ravier, M. A. *et al.* Loss of Connexin36 Channels Alters -Cell Coupling, Islet Synchronization of Glucose-Induced Ca^{2+} and Insulin Oscillations, and Basal Insulin Release. *Diabetes* **54,** 1798–1807 (2005).

82. Hayden, M. R. *et al.* Attenuation of Endocrine-Exocrine Pancreatic Communication in Type 2 Diabetes: Pancreatic Extracellular Matrix Ultrastructural Abnormalities. *J. Cardiometab. Syndr.* **3,** 234–243 (2008).

83. Rorsman, P. & Braun, M. Regulation of Insulin Secretion in Human Pancreatic Islets. *Annu. Rev. Physiol.* **75,** 155–179 (2013).

84. Lang, J. Molecular mechanisms and regulation of insulin exocytosis as a paradigm of endocrine secretion. *Eur. J. Biochem.* **259,** 3–17 (1999).

85. Eliasson, L. *et al.* Novel aspects of the molecular mechanisms controlling insulin secretion. *J. Physiol.* **586,** 3313–3324 (2008).

86. Bokvist, K., Holmqvist, M., Gromada, J. & Rorsman, P. Compound exocytosis in voltage-clamped mouse pancreatic beta-cells revealed by carbon fibre amperometry. *Pflugers Arch.* **439,** 634–645 (2000).

87. Grapengiesser, E., Gylfe, E. & Hellman, B. Glucose-induced oscillations of cytoplasmic Ca^{2+} in the pancreatic beta-cell. *Biochem. Biophys. Res. Commun.* **151,** 1299–1304 (1988).

88. Dryselius, S., Grapengiesser, E., Hellman, B. & Gylfe, E. Voltage-dependent entry and generation of slow Ca^{2+} oscillations in glucose-stimulated pancreatic beta-cells. *Am. J. Physiol.* **276,** E512–E518 (1999).

89. Bertram, R., Sherman, A. & Satin, L. S. Electrical Bursting, Calcium Oscillations, and Synchronization of Pancreatic Islets. *Adv. Exp. Med. Biol.* **654,** 261–279 (2010).

90. Stožer, A., Dolenšek, J. & Rupnik, M. S. Glucose-Stimulated Calcium Dynamics in Islets of Langerhans in Acute Mouse Pancreas Tissue Slices. *PLoS One* **8,** e54638 (2013).

91. Tengholm, A. & Gylfe, E. Oscillatory control of insulin secretion. *Mol. Cell. Endocrinol.* **297,** 58–72 (2009).

92. Gilon, P., Shepherd, R. M. & Henquin, J. C. Oscillations of secretion driven by oscillations of cytoplasmic Ca^{2+} as evidences in single pancreatic islets. *J. Biol. Chem.* **268,** 22265–22268 (1993).

93. Bergsten, P. Slow and fast oscillations of cytoplasmic Ca^{2+} in pancreatic islets correspond to pulsatile insulin release. *Am. J. Physiol.* **268,** E282–E287 (1995).

94. Fernandez, J. & Valdeolmillos, M. Synchronous glucose-dependent $[Ca^{2+}]_i$ oscillations in mouse pancreatic islets of Langerhans recorded in vivo. *FEBS Lett.* **477,** 33–36 (2000).

95. Dolenšek, J., Stožer, A., Skelin Klemen, M., Miller, E. W. & Slak Rupnik, M. The Relationship between Membrane Potential and Calcium Dynamics in Glucose-Stimulated Beta Cell Syncytium in Acute Mouse Pancreas Tissue Slices. *PLoS One* **8,** e82374 (2013).

96. Dolenšek, J. *et al.* Membrane Potential and Calcium Dynamics in Beta Cells from Mouse Pancreas Tissue Slices: Theory, Experimentation, and Analysis. *Sensors* **15,** 27393–27419 (2015).

97. Cigliola, V., Chellakudam, V., Arabieter, W. & Meda, P. Connexins and β-cell functions. *Diabetes Res. Clin. Pract.* **99,** 250–259 (2013).

98. Ravier, M. A. *et al.* Loss of connexin36 channels alters β-cell coupling, islet synchronization of glucose-induced Ca^{2+} and insulin oscillations, and basal insulin release. *Diabetes* **54,** 1798–1807 (2005).

99. Irles, E. *et al.* Enhanced glucose-induced intracellular signaling promotes insulin hypersecretion: Pancreatic beta-cell functional adaptations in a model of genetic obesity and prediabetes. *Mol. Cell. Endocrinol.* **404,** 46–55 (2015).

100. Notary, A. M., Westacott, M. J., Hraha, T. H., Pozzoli, M. & Benninger, R. K. P. Decreases in Gap Junction Coupling Recovers Ca^{2+} and Insulin Secretion in Neonatal Diabetes Mellitus, Dependent on Beta Cell Heterogeneity and Noise. *PLOS Comput.*

Biol. **12,** e1005116 (2016).

101. Speier, S., Gjinovci, A., Charollais, A., Meda, P. & Rupnik, M. Cx36-mediated coupling reduces β-cell heterogeneity, confines the stimulating glucose concentration range, and affects insulin release kinetics. *Diabetes* **56,** 1078–1086 (2007).

102. Head, W. S. *et al.* Connexin-36 Gap Junctions Regulate In Vivo First- and Second-Phase Insulin Secretion Dynamics and Glucose Tolerance in the Conscious Mouse. *Diabetes* **61,** 1700–1707 (2012).

103. Hodson, D. J. *et al.* Lipotoxicity disrupts incretin-regulated human β cell connectivity. *J. Clin. Invest.* **123,** 4182–4194 (2013).

104. Shield, J. & Summerbell, C. in *Obesity, Science and Practise* (eds. Williams, G. & Frühbeck, G.) 509–542 (2008).

105. Blondel, V. D., Guillaume, J.-L., Lambiotte, R. & Lefebvre, E. Fast unfolding of communities in large networks. *J. Stat. Mech. Theory Exp.* **2008,** P10008 (2008).

106. Valladolid-Acebes, I. *et al.* Spatial memory impairment and changes in hippocampal morphology are triggered by high-fat diets in adolescent mice. Is there a role of leptin? *Neurobiol. Learn. Mem.* **106,** 18–25 (2013).

107. Chen, Y. L. *et al.* Associations between genetic variants and the severity of metabolic syndrome in subjects with type 2 diabetes. *Genet. Mol. Res.* **14,** 2518–2526 (2015).

108. Romeo, S. *et al.* Search for genetic variants of the SYNTAXIN 1A (STX1A) gene: the -352 A>T variant in the STX1A promoter associates with impaired glucose metabolism in an Italian obese population. *Int. J. Obes.* **32,** 413–420 (2008).

109. Tsunoda, K., Sanke, T., Nakagawa, T., Furuta, H. & Nanjo, K. Single nucleotide polymorphism (D68D , T to C) in the syntaxin 1A gene correlates to age at onset and insulin requirement in Type II diabetic patients. *Diabetologia* **44,** 2092–2097 (2001).

110. Reinbothe, T. M. *et al.* The human L-type calcium channel Cav1.3 regulates insulin release and polymorphisms in CACNA1D associate with type 2 diabetes. *Diabetologia* **56,** 340–349 (2013).

111. Olson, T. M. & Terzic, A. Human K(ATP) channelopathies: diseases of metabolic homeostasis. *Pflugers Arch.* **460,** 295–306 (2010).

112. Morton, G. J., Meek, T. H. & Schwartz, M. W. Neurobiology of food intake in health and disease. *Nat. Rev. Neurosci.* **15,** 367–78 (2014).

113. Long, Y. C. & Zierath, J. R. Review series AMP-activated protein kinase signaling in metabolic regulation. *J. Clin. Invest.* **116,** 1776–1783 (2006).

114. Grahame Hardie, D. AMP-activated protein kinase: a key regulator of energy balance with many roles in human disease. *J. Intern. Med.* **276,** 543–559 (2014).

115. Friedman, J. 20 YEARS OF LEPTIN: Leptin at 20: an overview. *J. Endocrinol.* **223,** T1–T8 (2014).

116. Tanti, J.-F. & Jager, J. Cellular mechanisms of insulin resistance: role of stress-regulated serine kinases and insulin receptor substrates (IRS) serine phosphorylation. *Curr. Opin. Pharmacol.* **9,** 753–762 (2009).

117. Chatterjee, C. & Sparks, D. L. Hepatic Lipase, High Density Lipoproteins, and Hypertriglyceridemia. *Am. J. Pathol.* **178,** 1429–1433 (2011).

118. Müller, D. J. *et al.* The SNAP-25 gene may be associated with clinical response and weight gain in antipsychotic treatment of schizophrenia. *Neurosci. Lett.* **379,** 81–89 (2005).

119. Musil, R. *et al.* SNAP-25 gene polymorphisms and weight gain in schizophrenic patients. *J. Psychiatr. Res.* **42,** 963–970 (2008).

120. Perret, J., De Vriese, C. & Delporte, C. Polymorphisms for ghrelin with consequences on satiety and metabolic alterations. *Curr. Opin. Clin. Nutr. Metab. Care* **17,** 306–311 (2014).

121. Müller, T. D. & Tschöp, M. H. Ghrelin - A Key Pleiotropic Hormone-Regulating Systemic Energy Metabolism. *Ghrelin Syst.* **25,** 91–100 (2013).

122. Bruinstroop, E., Fliers, E. & Kalsbeek, A. Hypothalamic control of hepatic lipid metabolism via the autonomic nervous system. *Best Pract. Res. Clin. Endocrinol. Metab.* **28,** 673–684 (2014).

123. Lam, T. K. T. Neuronal regulation of homeostasis by nutrient sensing. *Nat. Med.* **16,** 392–395 (2010).

124. Satin, L. S., Butler, P. C., Ha, J. & Sherman, A. S. Pulsatile insulin secretion, impaired glucose tolerance and type 2 diabetes. *Mol. Aspects Med.* **42,** 61–77 (2015).

125. Rieck, S. & Kaestner, K. H. Expansion of beta-cell mass in response to pregnancy. *Trends Endocrinol. Metab.* **21,** 151–158 (2010).

126. Skelin, M. & Rupnik, M. cAMP increases the sensitivity of exocytosis to Ca^{2+} primarily through protein kinase A in mouse pancreatic beta cells. *Cell Calcium* **49,** 89–99 (2011).

127. Leung, Y. M. *et al.* Syntaxin 1A binds to the cytoplasmic C terminus of Kv2.1 to regulate channel gating and trafficking. *J. Biol. Chem.* **278,** 17532–17538 (2003).

128. MacDonald, P. E. *et al.* Synaptosome-Associated Protein of 25 Kilodaltons Modulates Kv2.1 Voltage-Dependent K^+ Channels in Neuroendocrine Islet β-Cells through an Interaction with the Channel N Terminus. *Mol. Endocrinol.* **16,** 2452–2461 (2002).

129. Yang, S.-N. *et al.* Syntaxin 1 interacts with the LD subtype of voltage-gated Ca^{2+} channels in pancreatic beta cells. *Proc. Natl. Acad. Sci.* **96,** 10164–10169 (1999).

130. Barabási, A.-L. The network takeover. *Nat. Phys.* **8,** 14–16 (2011).

131. Stožer, A. *et al.* Functional Connectivity in Islets of Langerhans from Mouse Pancreas Tissue Slices. *PLoS Comput. Biol.* **9,** e1002923 (2013).

132. Markovič, R. *et al.* Progressive glucose stimulation of islet beta cells reveals a transition from segregated to integrated modular functional connectivity patterns. *Sci. Rep.* **5,** 7845 (2015).

133. Gosak, M. *et al.* The relationship between node degree and dissipation rate in networks of diffusively coupled oscillators and its significance for pancreatic beta cells. *Chaos An Interdiscip. J. Nonlinear Sci.* **25,** 73115 (2015).

134. Johnston, N. R. *et al.* Beta Cell Hubs Dictate Pancreatic Islet Responses to Glucose. *Cell Metab.* **24,** 389–401 (2016).

135. Benninger, R. K. P. & Piston, D. W. Cellular communication and heterogeneity in pancreatic islet insulin secretion dynamics. *Trends Endocrinol. Metab.* **25,** 399–406 (2014).

136. Dulubova, I. *et al.* Munc18-1 binds directly to the neuronal SNARE complex. *Proc. Natl. Acad. Sci.* **104,** 2697–2702 (2007).

137. Betke, K. M. *et al.* Differential localization of G protein βγ subunits. *Biochemistry* **53,** 2329–2343 (2014).

138. García, D. E. *et al.* G-protein β-subunit specificity in the fast membrane-delimited inhibition of Ca^{2+} channels. *J Neurosci* **18,** 9163–9170 (1998).